Thermodynamics of Bivalent Heterotrimer Association in the Notch Signaling Pathway

Cyril Cook, Kristen M. Ramsey, and Doug Barrick

Abstract

The Notch signaling pathway regulates differentiation through a bivalent heterotrimer comprising the Notch intracellular domain (NICD), the DNA-binding protein CSL, and the coactivator MAML. NICD has two distinct sites for CSL: a short motif in the RAM region and an ankyrin domain (ANK). These two binding sites, connected by an intrinsically disordered linker, create a bivalent interaction with CSL. Here we use ITC to measure the thermodynamics of bivalent heterotrimer assembly. Although we are unable to detect heterodimer formation among ANK, MAML, and CSL pairs, titrations including all three proteins demonstrate cooperative heterotrimer formation. We have developed a heterotrimer model that fits the ITC data well.

By comparing subreactions involving different regions of RAMANK, we are able to quantify the thermodynamic contribution of bivalency to heterotrimer assembly. We find that bivalency increases occupancy of RAM and ANK binding to CSL *in cis* over binding to CSL *in trans* by about three orders of magnitude.

Introduction

Notch signaling is a signal transduction pathway that is central to cellular differentiation and homeostasis in metazoans, making major contributions to processes such as embryogenesis, wound healing, hematopoesis, neurogenesis, and stem cell maintenance [6, 36]. Genes comprising the Notch pathway were identified in genetic screens over a century ago [9]. Activation of Notch signaling is initiated by interaction of the Notch transmembrane receptor with ligands on adjacent cells, which triggers proteolysis of the Notch receptor, releasing the Notch intracellular domain (NICD) into the cytosol [22]. NICD is then imported into the nucleus, where it associates with CSL, a DNA-binding protein, and MAML, a co-activator; formation of this NICD:CSL:MAML ternary complex at promoters of Notch responsive genes activates their transcription [18]. Mutations in Notch signaling genes are associated with various cancers and diseases [1, 5].

Studies over the past 25 years using molecular genetics, biochemistry, and x-ray crystallography have highlighted several unique features of the Notch ternary complex [19]. Most notably, NICD engages CSL through two distinct regions, the RAM region (specifically a short ΦWΦP sequence motif[1] on the N-terminus of the RAM region) and the ANK domain, a highly conserved set of seven ankyrin repeats (Figure 1). The ΦWΦP motif of NICD binds to the β-trefoil domain (BTD) of CSL, whereas the ANK domain of NICD binds to the N- and C-terminal domains (NTD, CTD) of CSL. The distance between these two binding sites is

[1] Here Φ indicates hydrophobic residue

around 45 Å. The linker separating the ΦWΦP motif and the ANK domain is disordered both in solution and in the crystal structure [24, 34, 3]. X-ray crystallography shows that MAML binds to an extended interface between the ANK domain of NICD and the NTD and CTD domains of CSL as a long kinked α-helix [23, 34]. Biochemical studies show that the ANK domain and MAML region mutually stabilize one another in their interaction with CSL, and bind weakly (if at all) on their own [24].

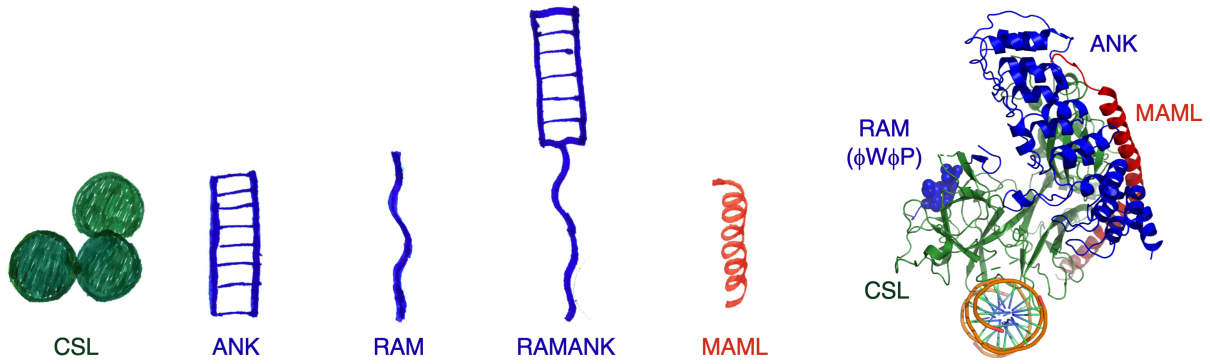

Figure 1: Cartoons of the polypeptides, regions, and domains that form the Notch transcriptional activation complex. Constructs used in this study, starting from the left: the three-domain CSL protein in green (residues 25-449), segments from the Notch intracellular domain in blue (ANK, residues 1858-2126; RAM, residues 1758-1888; RAMANK, residues 1758-2126), and the N-terminal helical binding motif of MAML in red (residues 8-76). Boundaries for the constructs used in this study are for human CSL, human Notch-1 and human MAML1. Right, crystal structure of the Notch1 RAMANK:CSL:MAML1:DNA complex from *C. elegans*, 2fo1.pdb.

The relevant segments of these three proteins for ternary complex formation are drawn in Figure 1, along with the crystal structure of the Notch transcription complex. We refer to the transcription complex formed from the RAMANK region of Notch, CSL, and MAML as "bivalent" because distant regions of NICD simultaneously bind distant sites on CSL. The importance of the bivalent interaction has been demonstrated in transcriptional activation assays in which higher levels of activation are achieved when RAM and ANK are physically connected on a single polypeptide, rather than on two separate polypeptides [15].

Here we determine the energetics of association of Notch RAM, ANK, and RAMANK (from the human Notch1 receptor) with MAML1 and CSL using isothermal titration calorimetry (ITC). The complexes that we have probed are shown in Figure 2. One of our goals is to analyze the thermodynamics of heterotrimer formation involving ANK and MAML binding to CSL. We show that under our ITC conditions, this complex is an obligate heterotrimer–none of the pairwise binary complexes (CSL:ANK, CSL:MAML, ANK:MAML) are populated to appreciable levels. We develop an analytical model that is capable of fitting ITC data where a single component (e.g., MAML) is titrated into a solution of the other two components (e.g., CSL and ANK). This provides, for the first time, a measure of the affinity of the CSL:MAML:ANK ternary complex. In addition to identifying concentrations under which this complex assembles, we can determine whether prebinding RAM to CSL *in trans* affects the free energy of binding for ANK and MAML to CSL, quantitatively testing the potential for allosteric coupling between these two binding sites. Moreover, by comparing the free energy of formation for the CSL:MAML:ANK ternary complex with the free energy of binding for the MAML and ANK domains to CSL *in cis* starting from a prebound RAMANK:CSL complex,

we quantify the free energy and enthalpy contribution of the bivalent linkage between RAM and ANK in binding to CSL. These comparisons provide an estimate of the effective concentration afforded by the disordered RAM linker, and reveal the extent to which bivalency promotes cooperative binding of RAM and ANK+MAML to CSL.

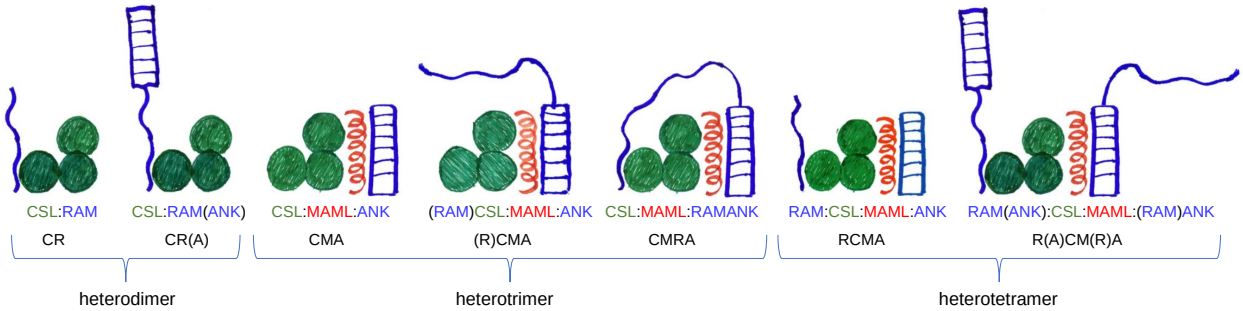

Figure 2: Complexes of CSL with the Notch RAM and ANK region, showing CSL bound both *in cis* and *in trans*, and the MAML binding motif. The acronyms at the bottom provide a shorthand for the reactions and binding data that follows. The two complexes on the left are dimeric complexes between RAM and CSL. Evidence below and from paralogue studies [26] indicates that the ANK domain does not bind to its site on CSL in the dimeric CSL:RAM(ANK) complex (second from left). In all heterotrimer and heterotetramer complexes, MAML stabilizes ANK binding to CSL. The rightmost heterotrimer (CMRA) displays RAMANK binding to CSL *in cis*, where two separate regions of a single NICD polypeptide engage CSL at two separate sites (comprising a bivalent interaction between RAMANK and CSL). The two heterotetramer complexes are different versions of both RAM and ANK binding to CSL *in trans*, meaning the RAM and ANK bound regions are from two separate polypeptides.

1 Results

In this study, we use ITC to measure the thermodynamics of a series of binding reactions in which parts of the bivalent CSL:RAMANK:MAML ternary complex are formed. Since many of these reactions can be viewed as steps in a larger thermodynamic cycle, comparing the thermodynamics of binding for various reactions allows us to answer questions related to allostery, cooperativity, and bivalency. To describe these complexes compactly and unambiguously, we use a shorthand nomenclature (Figure 2) in which single letters identify protein segments and domains (C for CSL, M for MAML1, R for Notch1 RAM, and A for the Notch1 ANK domain). For the RAMANK polypeptide, parenthesis indicate that a region or domain (RAM or ANK) is tethered to CSL but is not directly engaged with its binding site on CSL. For example, CR(A) indicates a dimeric complex where RAMANK is directly bound to CSL through its RAM region, but the ANK domain is dissociated (Figure 2).

With this framework, we can describe reactions that can be probed using ITC (Table 1):

Table 1: **Reaction definitions for CSL:RAMANK:MAML complexes**

#	Reaction	K	ΔG°
1	$C + R \rightleftharpoons CR$	K_{CR}	ΔG°_{CR}
2	$C + RA \rightleftharpoons CR(A)$	$K_{CR(A)}$	$\Delta G^\circ_{CR(A)}$
3	$C + A \rightleftharpoons CA$	K_{CA}	ΔG°_{CA}
4	$C + M \rightleftharpoons CM$	K_{CM}	ΔG°_{CM}
5	$M + A \rightleftharpoons MA$	K_{MA}	ΔG°_{MA}
6	$C + M + A \rightleftharpoons CMA$	K_{CMA}	ΔG°_{CMA}
7	$CR + M + A \rightleftharpoons RCMA$	K_{RCMA}	ΔG°_{RCMA}
8	$CR(A) + M \rightleftharpoons CMRA$	K_{cis}	ΔG°_{cis}
9	$CR(A) + M + RA \rightleftharpoons R(A)CM(R)A$	K_{tetra}	ΔG°_{tetra}

The first five reactions are bimolecular, whereas the next two (reactions 6-7) are termolecular. Reaction 8, where MAML binds to a complex in which RAMANK is prebound to CSL (CR(A)), is analogous to reaction 6, but the ANK domain binds to CSL *in cis*. Thus, reaction 8 is bimolecular. Reaction 9 starts with the same prebound CR(A) complex as reaction 8, but the ANK binding to CSL is *in trans* rather than *in cis*. Thus reaction 9 is termolecular. The experimental setup used to characterize reactions 1-7 by ITC is shown in Table 2, indicating which protein is in the syringe and which protein (or proteins, for reactions 6 and 7) are in the cell.

Table 2: **ITC experiments to dissect CSL:RAMANK:MAML assembly thermodynamics**

#	Rxn	Syringe	Cell	ΔG°	ΔH°
1	$C + R \rightleftharpoons CR$	RAM	CSL	$\Delta G^\circ_{CR} = -10.2 \pm 0.1$	$\Delta H^\circ_{CR} = -19.9 \pm 0.3$
2	$C + RA \rightleftharpoons CR(A)$	RAMANK	CSL	$\Delta G^\circ_{CR(A)} = -10.5 \pm 0.1$	$\Delta H^\circ_{CR(A)} = -19.0 \pm 0.2$
3	$C + A \rightleftharpoons CA$	ANK	CSL	n.d.	n.d.
4	$C + M \rightleftharpoons CM$	MAML	CSL	n.d.	n.d.
5	$M + A \rightleftharpoons MA$	MAML	ANK	n.d.	n.d.
6	$C + M + A \rightleftharpoons CMA$	MAML	CSL + ANK	$\Delta G^\circ_{CMA} = -17.9 \pm 0.1$	$\Delta H^\circ_{CMA} = -31.3 \pm 0.3$
7	$CR + M + A \rightleftharpoons RCMA$	MAML	CR + ANK	$\Delta G^\circ_{RCMA} = -18.2 \pm 0.1$	$\Delta H^\circ_{RCMA} = -26.7 \pm 0.3$

Titrations were performed at 25 °C in 200 mM NaCl, 0.5 mM TCEP, 25 mM Na_2HPO_4, pH 7.0. For reactions 3-5, ITC . thermograms show small heats that remain constant over the course of the titration, providing no evidence of binding. Units of ΔG° and ΔH° are kcal/mol. Errors are standard deviations on the mean from three technical replicates.

For bimolecular reactions 1-5 there is a single polypeptide in the cell and another in the syringe. For termolecular reaction 6 there are two different polypeptides in the cell which do not assemble in isolation. For reaction 7 there are three polypeptides in the cell, but the reaction is termolecular because RAM binds

tightly to CSL (and is at stoichiometric excess) prior to injection of MAML.

1.1 RAM binds CSL robustly and independently of ANK

The RAM region of Notch has long been recognized to form a stable binary complex with CSL in solution. This interaction was first identified through yeast two-hybrid and *in vitro* pull-down experiments by Honjo and coworkers [31]. Nam and coworkers mapped the interaction to the central BTD domain of CSL [24]. Kovall and Hendrickson identified a putative binding site for the ΦWΦP motif of RAM on the BTD domain of a crystal structure of CSL from *C. elegans* [20]. ITC studies showed a robust interaction between a peptide spanning the ΦWΦP motif and the BTD domain of CSL [21]; alanine-scanning mutagenesis showed the ΦWΦP motif to be a major determinant of binding energetics, with modest contributions from moderately conserved nearby residues [16]. Subsequent ITC showed that the RAM region binds to larger CSL constructs containing all three domains (NTD, BTD, CTD) with similar, albeit slightly higher affinities than to the isolated BTD domain [11, 29].

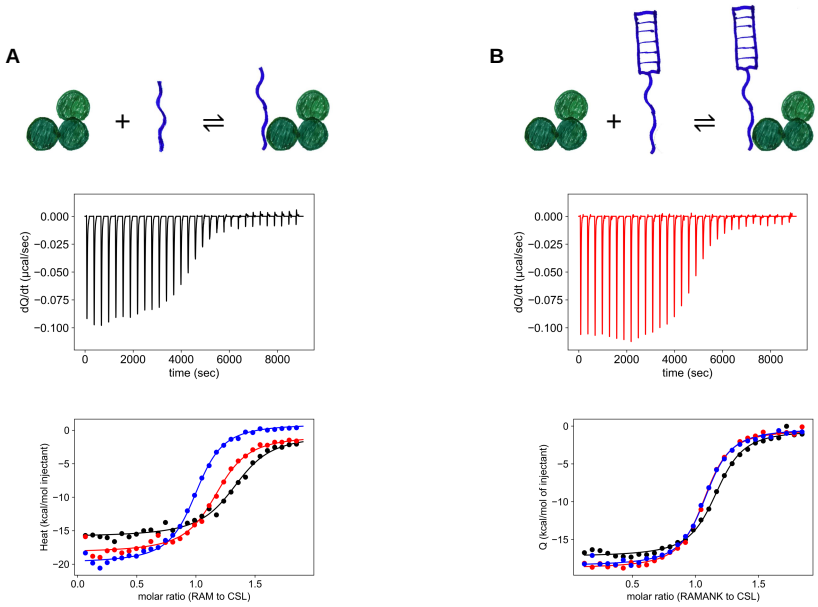

Figure 3: Binding of RAM and RAMANK to CSL measured by ITC. (A) RAM, and (B) RAMANK titrated into 2 μM CSL. Middle panels show baseline-corrected thermograms. Bottom panels show integrated heat values from each injection. The three curves for the RAM titrations (A) are replicate titrations at 20, 23.5, and 27 μM RAM in the syringe (black, red, and blue). The three curves for the RAMANK titrations (B) are replicate titrations each at 20 μM RAMANK in the syringe. The lines show a global fit of the three curves; ΔG° and ΔH° values are fitted globally, whereas heats of dilution and competent ligand fractions are fitted locally. Competent fractions for RAM (A) are 76, 75, and 77 percent (black, red, and blue) and for RAMANK (B) are 89, 97, and 96 percent (black, red, and blue).

The binding of human Notch1 RAM to human CSL by ITC is shown in Figure 3A. As with previous studies, the integrated heats associated with each injection are well-fitted by a heterodimer association model. The model includes an adjustable parameter for the fraction of incompetent material in the injection syringe.

The value of ΔG°_{CR} determined from a global fit of the three curves in Figure 3A (-10.2 ± 0.1 kcal/mol) is close to previously reported values (-10.5 kcal/mol from [29], and -10.4 kcal/mol using murine proteins from [11]).

The binding of RAMANK to CSL is shown in Figure 3B. Again, data are well-fitted by a heterodimer association model. The value of $\Delta G^{\circ}_{CR(A)}$ determined from global fit from the three curves in Figure 3B (-10.5 ± 0.1 kcal/mol) is close to a previously reported value (-10.7 kcal/mol from [28]). Moreover, fitted $\Delta G^{\circ}_{CR(A)}$ and $\Delta H^{\circ}_{CR(A)}$ values for RAMANK (Figure 3B) are nearly identical to ΔG°_{CR} and ΔH°_{CR} values for RAM (Figure 3A), suggesting that the ANK domain does not interact with CSL when it is tethered to RAM in the absence of MAML. This interpretation is consistent with studies of chimeric human RAMANK orthologues interacting with CSL, which indicate that RAMANK binding to CSL is insensitive to the identity of the ANK domain [26]. Although it is possible that the modest decrease in $\Delta G^{\circ}_{CR(A)}$ compared to $\Delta G^{\circ}_{CR} =$ (-10.5 versus -10.2 kcal/mol, Table 2) and a similar enhancement reported in both [4] and [29] reflects a weak CSL-ANK interaction when ANK is tethered *in cis* through RAM, these differences are small, and nearly within error.

1.2 Neither ANK nor MAML bind detectably to CSL

In contrast to the robust interaction of RAM with CSL, neither Notch1 ANK nor the MAML1 binding region shows evidence of forming a heterodimeric complex with CSL on their own, showing small uniform heat peaks when titrated to a two-fold molar excess relative to CSL (Figure 4A,B). Since these peaks are similar in profile and magnitude to peaks obtained when water is injected into water (Figure 4D), these peaks are likely to be heats of injection.

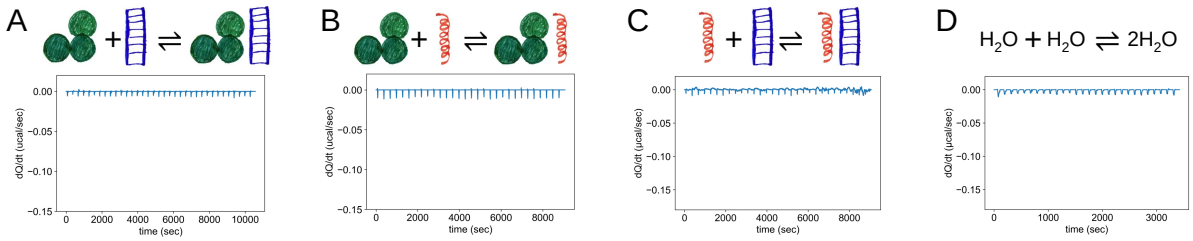

Figure 4: ITC cannot detect formation of binary complexes from ANK, MAML, and CSL. (A) $2\mu M$ CSL titrated with $20\mu M$ ANK. (B) $2\mu M$ CSL titrated with $20\mu M$ MAML. (C) $2\mu M$ MAML titrated with $20\mu M$ ANK. (D) Titration of water into water. Plots show baseline corrected thermograms.

Similarly, small uniform heat peaks are obtained when the Notch1 ANK domain is titrated with MAML1 to a two-fold excess, suggesting that Notch1 ANK and MAML do not interact in isolation (Figure 4C). These results are consistent with findings from Nam and coworkers [24] that suggest that human Notch1 ANK and MAML1 bind weakly to CSL in isolation. In contrast, Kovall and coworkers were able to detect binding of Drosophila Notch ANK domain to Suppressor of Hairless (the Drosophila CSL orthologue) by ITC, with a ΔG°_{CA} value of -8.4 kcal/mol (a K_d of 0.7 μM) [8], suggesting there may be considerable variation in affinity among orthologues.

1.3 CSL + ANK + MAML form a robust complex

We showed in Figure 4A that titration of CSL with ANK gives no heat peaks, but a titration of CSL and MAML with ANK does give clearly discernible heat peaks (Figure 5A). Similarly, Figure 4B showed that CSL titrated with MAML yields no heat peaks; but titrations of CSL and ANK with MAML yield heat peaks (Figure 5B). Titrations of CSL with either ANK or MAML result in no heat peaks, and titrations of MAML with ANK give no heat peaks (4C), but titrations of both MAML and ANK with CSL give heat peaks (Figure 5C). Titrations involving all three proteins (CSL, ANK, and MAML) result in heat peaks regardless of which protein is in the syringe of the calorimeter (as can be seen by comparing Figure 5A, Figure 5B, and Figure 5C.) This provides strong evidence for higher-order complex formation.

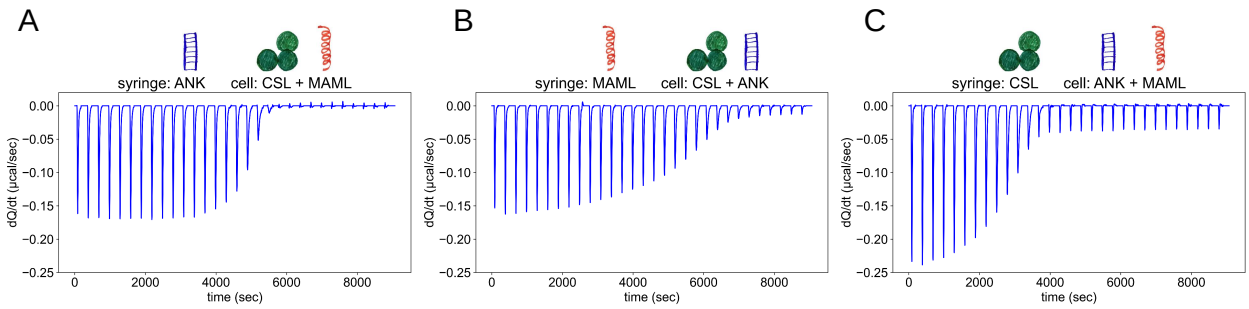

Figure 5: ITC can detect formation of ternary complexes from ANK, MAML, and CSL. (A) $2\mu M$ CSL and $35\mu M$ MAML titrated with $20\mu M$ ANK. (B) $2\mu M$ CSL and $8\mu M$ ANK titrated with $20\mu M$ MAML. (C) $2\mu M$ ANK and $8\mu M$ MAML titrated with $20\mu M$ CSL. Upper cartoons show positions of proteins in ITC experiment setup. Bottom panels show baseline corrected thermograms.

1.4 A model for studying obligate heterotrimer formation by ITC

Lack of heterodimer formation among CSL, ANK, and MAML (Figure 4) and formation of heat peaks during titrations with all three proteins regardless of which protein is in the calorimeter syringe (Figure 5) suggests that the CSL:MAML:ANK ternary complex is an obligate ternary complex, in which MAML and ANK stabilize one another in their interaction with CSL. To analyze the thermodynamics of CSL:MAML:ANK ternary complex formation, a model is needed that expresses the amount of ternary complex formed in each injection. As with binary complex formation, the heat associated with the ith injection is equal to the number of moles of CMA (CSL-MAML-ANK) complex formed as a result of injection, n_i, times the molar enthalpy of complex formation:

$$q_i = \Delta H_{CMA} \times (n_i - n_{i-1}) \tag{1}$$

$$= \Delta H_{CMA} \times V_{cell} \times ([CMA]_i - [CMA]_{i-1}) \tag{2}$$

In equation 2, the number of moles of complex is expressed using the product of the molarity ($[CMA]$) and cell volume (V_{cell}).

In principle, the molarity of CMA can be determined from the equilibrium constant, which is logarith-

mically related to the free energy for formation of CMA (ΔG°_{CMA}). Rearranging the mass-action expression for K_{CMA} gives

$$[CMA] = K_{CMA}[C][M][A] \tag{3}$$

However, none of the free concentrations on the right-hand-side of equation 3 are known (nor is the equilibrium constant, which is to be determined in a fit to the data). A more useful equation can be obtained by replacing the unknown free concentrations $[C]$, $[M]$, and $[A]$ with the total concentrations of each species, which are known[2]. For each species, the free concentration is equal to the total concentration minus the concentration of the ternary complex (e.g., for MAML, $[M] = [M]_t - [CMA]$). Replacing each concentration term in equation 3 gives

$$[CMA] = K_{CMA}([C]_t - [CMA])([M]_t - [CMA])([A]_t - [CMA]) \tag{4}$$

Equation 4 provides a relationship between the concentration of the ternary complex, $[CMA]$, and the equilibrium constant, using known total concentrations. However, this equation does not have an explicit form needed for fitting (i.e., $[CMA] = f(K_{CMA}, [C]_t, [M]_t, [A]_t)$. Rather, equation 4 is cubic in $[CMA]$. Although the cubic equation has an analytical solution, compared to the quadratic equation associated with heterodimer formation, the solution to the cubic equation is quite lengthy and presents some challenges for fitting. A workable solution that generates values of $[CMA]_i$ (the concentration of the ternary complex after the ith injection) as an explicit function of K_{CMA} and the starting concentrations ($[C]_0$, $[M]_0$, and $[A]_0$) is presented in Appendix 1. This solution can be inserted into equation 2, which can be fitted to the integrated heats of injection using nonlinear least squares.

1.5 CSL, ANK, and MAML bind robustly as an obligate heterotrimer

In principle, heterotrimer formation among CSL, ANK, and MAML can be measured through six different experimental setups. As demonstrated in Figure 5, any two proteins can be put in the calorimetry cell, and the third protein can be placed in the syringe. Practical considerations favor some setups over others. Because proteins in the syringe need to be at a significantly higher concentration (typically ten-fold molar excess) than proteins in the cell, we chose to put two proteins in the cell and one in the syringe to conserve material (Figure S1A). Since CSL is challenging to prepare at high concentrations compared to ANK and MAML, we put CSL in the cell as the limiting cell ligand. We initially included MAML in the cell at stoichiometric excess to CSL (the excess cell ligand), but during the course of these experiments we learned that the fraction of binding-competent MAML is variable compared to fractions of binding-competent CSL and ANK. Because accurate determination of the incompetent fraction is important to accurately determine binding energetics, and because the incompetent fraction of the excess cell ligand cannot be accurately determined because it has no effect upon the observed molar ratio of syringe ligand to limiting cell ligand (compare Figure S1B,C to S1D), we switched MAML to the syringe. Using this experimental configuration we could accurately fit the energetics of ternary complex formation, without confounding effects from uncertainties in MAML binding

[2] More precisely, the initial concentrations of the proteins in the cell ($[C]_0$, $[A]_0$) and syringe ($[M]_0$) are known. Total concentrations after injection i are decreased from initial values by dilution and displacement associated with each injection. The conversion from initial concentrations to total concentrations is provided in Appendix 1.

competency.

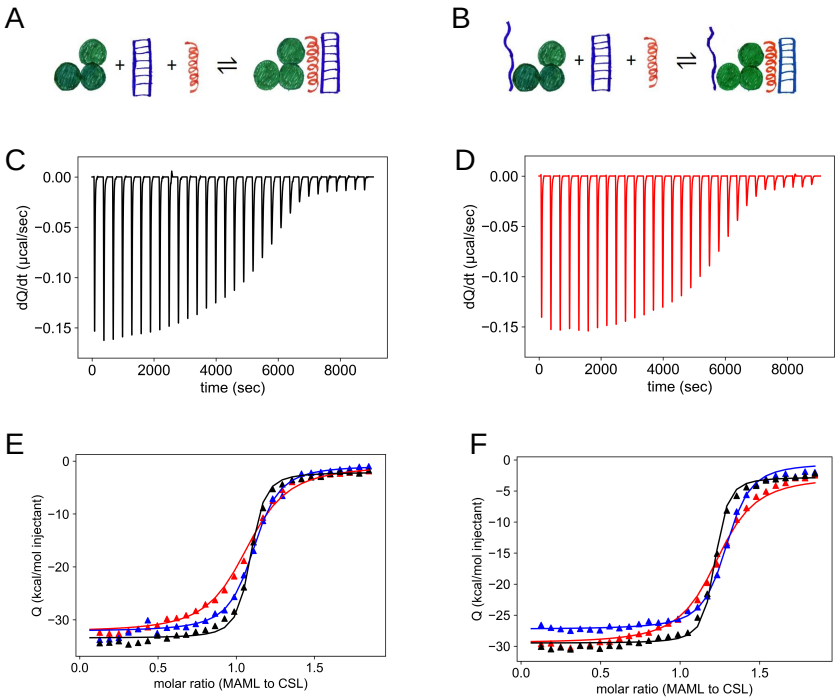

Figure 6: Ternary complex formation involving CSL, ANK, and MAML. Panel (A) shows the proteins being titrated for panels (C) and (E), and panel (B) shows the same for panels (D) and (F). Panels (C) and (D) show baseline-corrected thermograms. In both (C) and (D), $2\mu M$ CSL and $8\mu M$ ANK in the cell are titrated with $20\mu M$ MAML in the syringe. In (D) the cell also contains $10\mu M$ RAM (*in trans* to ANK), a five-fold stoichiometric excess to CSL. At these concentrations and experimental conditions, CSL should be 99.75 percent saturated with RAM. Panel (C) had 78% binding competent MAML, and panel (D) had 76% binding competent MAML. Panels (E) and (F) each show integrated heats of injection for three titrations, wherein both have $20\mu M$ MAML in the syringe, $2\mu M$ CSL in the cell, and $4\mu M$ (red), $8\mu M$ (blue), or $22\mu M$ (black) ANK respectively. Additionally, Panel (F) has $10\mu M$ (red, blue, and black) RAM in the cell. MAML competent fractions in (E) are 95% (red), 94% (blue), and 96% (black). MAML competent fractions in (F) are 82% (red), 80% (blue), and 85% (black). Solid lines are global fits using the obligate heterotrimer model (equation 2).

A titration of MAML into CSL and ANK is shown in Figure 6C. At least superficially, the shape of the integrated heat profile resembles that of heterodimer formation. To demonstrate that the heat peaks in this titration result from heterotrimer formation, we collected titrations at the same MAML and CSL concentrations but varying ANK (the excess cell ligand) concentrations (Figure 6E). The titrations at higher ANK concentrations have similar overall heats and midpoints, but steeper transitions. As shown in Figure S1D, this increase in steepness as the excess cell ligand concentration increases is expected for obligate heterotrimer formation. This sensitivity to the concentration of the excess cell ligand, along with the observation that CSL, ANK, and MAML are unable to form heterodimeric species, supports an obligate heterotrimer mechanism for titrations of CSL, ANK, and MAML (Table 1, reaction 6).

The heterotrimer model fits well to the individual titrations of MAML into CSL and ANK . To more

accurately determine ΔG°_{CMA} and ΔH°_{CMA}, we globally fit the heterotrimer model to three ITC experiments with different ANK concentrations. The global fit accurately reproduces the three titrations, and captures the increase in slope that results from increasing the total concentration of the excess ligand ANK in the calorimeter cell (curves, Figure 6E).

The free energy and enthalpy of formation for the ternary complex between CSL, MAML, and ANK obtained from this global fit ($\Delta G^{\circ}_{CMA} = -17.9$ and $\Delta H^{\circ}_{CMA} = -31.3$ kcal/mol, Table 2, reaction 6) are considerably larger in magnitude than typical values for bimolecular protein-protein interactions (e.g. $\Delta G^{\circ}_{CR(A)} = -10.5$ kcal/mol and $\Delta H^{\circ}_{CR(A)} = -19.0$ kcal/mol). The large negative enthalpy is not surprising, given the considerable surface area that is buried in the CSL:MAML:ANK ternary complex (7,663 $\AA^2$) [10, 7], and the coil-to-helix transition that is likely to accompany MAML binding [27]. The buried surface area can be used to calculate the heat capacity change expected for CSL-ANK-MAML association [13]. This calculated value ($\Delta Cp_{CMA} = -1.58$ kcal/mol K) is close to an experimental value ($\Delta Cp_{CMA} = -1.46$ kcal/mol K) we determined from fitting the temperature dependence of ΔH°_{CMA} (Figure S2). This agreement is further evidence that the complex formed in titrations of MAML into CSL and ANK is heterotrimeric.

The large negative free energy for ternary complex formation is due, in part, to the stoichiometry of the reaction, which involves three unbound reactants (CSL, MAML, and ANK). ΔG°_{CMA} is the free energy of reaction at the standard state, which is defined as one molar concentrations of reactants and products. At this high (and highly unphysiological) standard-state, the 3:1 stoichiometry provides strong driving force to form the ternary complex. However as described in the discussion, at concentrations of CSL, MAML, and ANK closer to those used in the ITC experiments, the value of ΔG_{CMA} increases to a more commonly-encountered, yet still favorable, value.

1.6 Binding of RAM and MAML+ANK to CSL are uncoupled

The binding of RAM to the BTD of CSL has been proposed to allosterically enhance the binding of ANK and MAML to the NTD and CTD of CSL, based on structural crystallographically-observed structure changes as well as gel-shift assays [11]. The ability to measure the free energy of ANK-MAML interaction with CSL provides a direct way to quantify the thermodynamics of this proposed allosteric coupling, by pre-forming the RAM:CSL complex and measure the free energy of MAML-ANK binding (reaction 7, Table 1) using the ternary fitting model described above. If RAM binding to CSL enhances the ANK-MAML interaction, the standard state free energy of binding ANK and MAML to the pre-formed RAM:CSL complex should be more negative than that for forming the ternary CMA complex in the absence of RAM (reaction 6, Table 1).

Titration of CSL (prebound with RAM) and ANK with MAML (reaction 7, Table 2) produces a heat profile very similar to the analogous titration in the absence of RAM ((reaction 6, Table 2); compare Figures 6C,E and D,F). In these titrations, the cell contains 2 μM CSL, 10 μM RAM, and varying concentrations of ANK. Based on the free energy of RAM-CSL binding (Table 2, reaction 1), CSL should be 99.8 percent bound with RAM at these concentrations. Globally fitting the data in Figure 6F with the model for obligate ternary complex formation gives a very similar free energy (-18.2 kcal/mol) to that fitted for heterotrimer association without RAM (-17.9 kcal/mol) (Table 2). This result indicates that the binding of MAML and ANK to CSL are not thermodynamically coupled to the binding of RAM in the absence of the covalent linkage between RAM and ANK. These results appear to be at odds with previous results from Friedmann

and Kovall using gel-shift assays that show that MAML and ANK bind more readily to CSL in the presence of RAM [11]. One difference between these two studies is that the present study uses human proteins whereas the Friedmann study used *C. elegans* and mouse proteins. Another difference is that in the Friedmann study, CSL was bound to DNA. It is possible that coupling between the RAM- and MAML-ANK binding sites on CSL is mediated by bound DNA.

1.7 Binding of ANK and MAML to CSL *in cis* and the energetics of bivalency

The ability to separate the CSL:RAM and CSL:ANK:MAML interactions (Table 2 reactions 1, 2, and 6) and quantify their binding energies provides a means to extract the contribution of bivalency from the overall assembly energy of the bivalent ternary complex (CMRA in Figure 1). Since the binding of RAM and ANK/MAML to CSL *in trans* seem to be uncoupled (Figure 6), the binding energy of the bivalent ternary complex is equal to the sum of the separate CR(A) and CMA binding energies plus the free energy of bivalent coupling between the two (ΔG°_φ), i.e.,

$$\Delta G^\circ_{CMRA} = \Delta G^\circ_{CR(A)} + \Delta G^\circ_{CMA} + \Delta G^\circ_\varphi \tag{5}$$

A simple way to measure the free energy of bivalent coupling is to compare the assembly energy of the ternary CSL:MAML:ANK complex (reaction 6, Table 2) with the analogous reaction starting from a prebound CSL:RAMANK complex (reaction 8, Table 3).

Table 3: **ITC experiments to dissect energetics of bivalency**

#	Rxn	Syringe	Cell	ΔG°	ΔH°
8	$CR(A) + M \rightleftharpoons CMRA$	MAML	CR(A)	$\Delta G^\circ_{cis} = -11.6 \pm 0.1$	$\Delta H^\circ_{cis} = -28.3 \pm 0.3$
9	$CR(A) + M + RA \rightleftharpoons CMRA + R(A)CM(R)A$	MAML	CR(A)	$\Delta G^\circ_\varphi = 6.4 \pm 0.2$	$\Delta H^\circ_\varphi = 9.1 \pm 1.4$

Titrations were performed at 25 °C in 200 mM NaCl, 0.5 mM TCEP, 25 mM Na_2HPO_4, pH 7.0. Units of ΔG° and ΔH° . are kcal/mol. Errors are standard error on the mean from at least three technical replicates.

Thus, the binding energy of MAML to the prebound CR(A) complex should include the contribution from binding of ANK, since ANK does not appear to be bound in the CR(A) complex (Figure 3). The free energy of MAML binding to CR(A) *in cis* is equal to the assembly energy of the CMA complex plus the free energy of bivalent coupling, ΔG°_φ:

$$\Delta G^\circ_{cis} = \Delta G^\circ_{CMA} + \Delta G^\circ_\varphi \tag{6}$$

Rearranging this equation leads to an experimentally accessible definition of the free energy of bivalent coupling:

$$\Delta G^\circ_\varphi = \Delta G^\circ_{cis} - \Delta G^\circ_{CMA} \tag{7}$$

Similarly, the enthalpy of bivalent coupling is

$$\Delta H^{\circ}_{\varphi} = \Delta H^{\circ}_{cis} - \Delta H^{\circ}_{CMA} \tag{8}$$

Five titrations of CSL prebound by RAMANK (CR(A)) with MAML are shown in Figure 7. These titrations differ in the amount of RAMANK in the cell along with $2\,\mu M$ CSL, though in all cases, RAMANK is in excess of CSL and should be sufficient to fully saturate the CR(A) complex. Unlike the titration of CSL + ANK with MAML (reaction 6, Figure 6), the five heat profiles all have the same slope, consistent with the expected heterodimer mechanism.

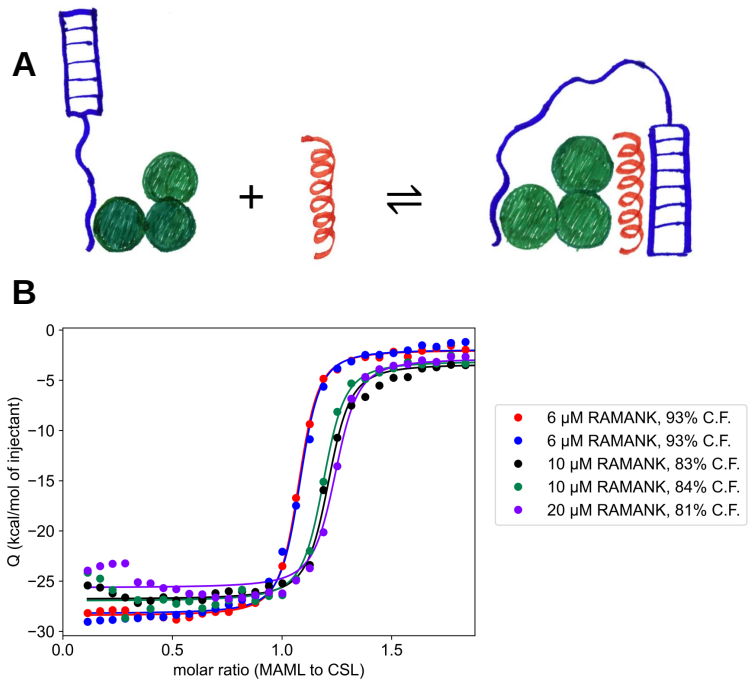

Figure 7: Binding of MAML and the ANK domain *in cis* to CSL, using a heterodimer model to determine ΔG°_{cis}. Panel (A) shows the reaction being considered, in which MAML is titrated into CSL prebound with RAMANK. Panel (B) shows integrated heats of injection from five titrations with RAMANK at concentrations varying from $6\mu M$ to $20\,\mu M$ prebound to $2\,\mu M$ CSL in the ITC cell, titrated with $20\,\mu M$ MAML (locally fitted binding competent fractions of MAML are abbreviated as C.F. above). At these concentrations, CSL should be $> 99\%$ percent saturated with RAMANK. Curves are from globally fitting the data for ΔG°_{cis} and ΔH°_{cis} using the heterodimer model shown in (A).

Globally fitting the data in Figure 7 to a bimolecular association scheme leads to an estimate of ΔG°_{cis} of -11.6 kcal/mol and ΔH°_{cis} of -28.3 kcal/mol. Combining these values with the free energy and enthalpy of forming the ternary complex (reaction 6, Table 2) with equations 7 and 8 gives the free energy and enthalpy of bivalent coupling ($\Delta G^{\circ}_{\varphi}$ and $\Delta H^{\circ}_{\varphi}$) of $+6.3$ kcal/mol and $+3.0$ kcal/mol. Although the positive value of $\Delta G^{\circ}_{\varphi}$ might seem to suggest an energetically unfavorable reaction, this interpretation is complicated by the stoichiometry difference between reactions 6 and 8 and the use of a one molar standard state. As developed below, at dilute (physiologically relevant) concentrations, this value of $\Delta G^{\circ}_{\varphi}$ produces considerable coupling between RAM and ANK/MAML binding to CSL.

1.8 A more complete model to determine the energetics of bivalency

In addition to forming the bivalent ternary (CMRA) complex, the MAML titrations of CSL prebound with RAMANK (Figure 7) have the potential to form a tetrameric complex containing two RAMANK molecules (R(A)CM(R)A, Figure 2). This tetrameric complex, which would be favored at high RAMANK concentrations[3], is not accounted for in the model used to fit ΔG°_{cis} in the previous section. Neglecting tetramer formation could adversely affect fitted parameters, in particular, the parameters associated with bivalency ($\Delta G^{\circ}_{\varphi}$ and $\Delta H^{\circ}_{\varphi}$).

Here we develop a fitting model that includes all species that can form in a mixture of CSL, RAMANK, and MAML, including CR(A), CMA, and R(A)CM(R)A, in addition to the bivalent ternary complex (CMRA). Derivation of an analytical fitting equation that includes the tetrameric species is significantly complicated by the quartic equation that results from expression of K_{tetra} in terms of total concentrations. Instead, we have developed a routine that uses numerical methods to solve for the unbound concentrations needed to fit the ITC data with nonlinear least squares (Appendix 3). This approach is based on that of Vega et al. [33]. To simplify analysis, we fixed ΔG° and ΔH° for CR(A) and CMA at values determined in Figures 3 and 6 (Table 2), and fit $\Delta G^{\circ}_{\varphi}$ and $\Delta H^{\circ}_{\varphi}$ in titrations of preformed CR(A) complexes with MAML (Figure 8).

[3] Assuming $\Delta G^{\circ}_{tetra} = \Delta G^{\circ}_{CMA} + \Delta G^{\circ}_{CR(A)}$, the estimate of $\Delta G^{\circ}_{\varphi}$ from ΔG°_{cis} (Figure 7) can be used to calculate the relative amounts of bivalent ternary and tetrameric complexes (see Appendix 2). At $6\mu M$ free RAMANK and $3\mu M$ free MAML, CSL should form 77% bivalent ternary complex and 23% tetrameric complex.

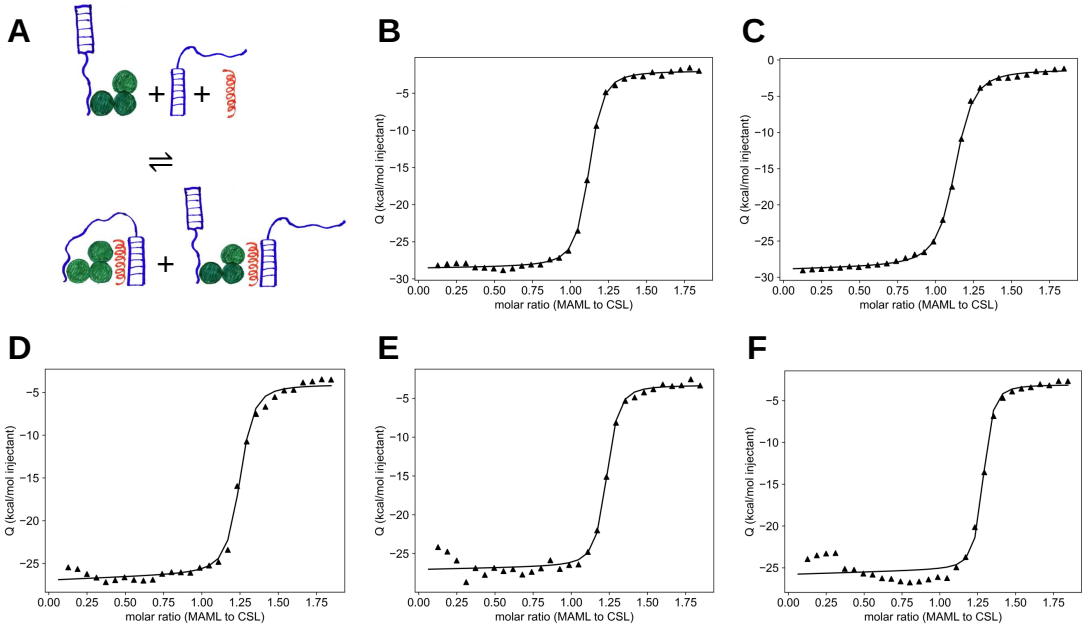

Figure 8: Numerical fitting to determine $\Delta G^{\circ}_{\varphi}$ from titrations of prebound CSL:RAMANK with MAML. (A) Highest-populated ligation states during the experiment. In all five titrations, MAML is in the syringe at $20\mu M$, and CSL is in the cell at $2\mu M$ with a molar excess of RAMANK at $6\mu M$ (B and C), $10\mu M$ (D and E), and $20\mu M$ (F). At these concentrations, CSL should be > 99.8 percent saturated with RAMANK. Fitted binding competent fractions of MAML are 93%, 93%, 83%, 84%, and 80% (B-F). Curves are the result of numerical fits for $\Delta G^{\circ}_{\varphi}$ and $\Delta H^{\circ}_{\varphi}$ (Appendix 3).

Five titrations of CSL prebound with different concentrations of saturating RAMANK with MAML are shown in Figure 8. Individually fitting each curve using the numerical solution described in Appendix 3 gives a $\Delta G^{\circ}_{\varphi}$ value of $+6.4 \pm 0.2$ kcal/mol and a $\Delta H^{\circ}_{\varphi}$ value of $+9.1 \pm 1.4$ kcal/mol (Table 3). This value of $\Delta G^{\circ}_{\varphi}$ is within error of the value determined using equations 7 and 8 (Figure 7). However, there is a significant change in $\Delta H^{\circ}_{\varphi}$, which increases from 3.0 to 9.1 kcal/mol when tetramer is accounted for. This change in the value of $\Delta H^{\circ}_{\varphi}$ leads to a favorable entropy of bivalency (+9.1 cal/mol K).

2 Discussion

The assembly of the Notch transcriptional activation complex is a critical step in the Notch signaling pathway, and is essential for development and homeostasis. The bivalent interaction between the RAM and ANK regions of the Notch intracellular domain and CSL has been appreciated for more than two decades, first from functional and pull-down studies and then from structural studies [14, 24, 4]. Transcriptional activation studies have shown that maximal activity requires RAM and ANK on the same polypeptide, as opposed to being on two separate polypeptides incapable of the bivalent interaction [15]. The mechanisms underlying bivalency have been discussed extensively, and include allosteric coupling between the RAM and ANK binding sites [11], and an effective concentration enhancement by which binding of RAM (or ANK via MAML) increases the local concentration of ANK (or RAM) near its site on CSL [3]. There has been

some support for enhancement of effective concentration from deletion and insertion studies studies within the linker [30], but experimental determination of the thermodynamic contributions of bivalency and the magnitude of the effective concentration enhancement have been lacking. By developing an ITC assay to measure ternary complex formation along with an equation for data analysis, we have been able to provide the experimental thermodynamic quantities needed to determine the effective concentration enhancement.

2.1 The free energy of CSL:MAML:ANK ternary complex formation and the one molar standard state

Although none of the pairwise interactions among CSL, MAML, and ANK can be detected at ITC concentrations ($2-10\,\mu M$), a robust and saturable complex is formed at an approximate 1:1:1 stoichiometry when all three proteins are combined, regardless of which protein is in the syringe and which proteins are in the calorimeter cell (Figure 5). Injection heats are well-fitted by a model for ternary complex formation, and show the expected sensitivity to the concentration of the excess cell ligand (Figure 6).

As mentioned above, the free energy for formation of the CSL:MAML:ANK ternary complex ($\Delta G^{\circ}_{CMA} = -17.9$ kcal/mol) is larger in magnitude than values typically measured in the ITC for bimolecular association. Despite this large value, the titration is shallow enough in the transition region to detect and quantify measurable equilibrium between the ternary complex and the dissociated proteins, as is seen for heterodimer reactions with smaller free energies of binding (see Figure 3 for example).[4] This difference in free energy is largely a result of the difference between the stoichiometry of the reaction, and the fact that free energies are reported at a one molar standard state.

Although a concentration of one molar reactants and products would strongly favor the termolecular association of CMA due to its 3-to-1 stoichiometry, the free energy falls dramatically as concentration decreases. For example, at concentration of one micromolar reactants and products (i.e., $[C] = [M] = [A] = [CMA] = 1\mu M$), the free energy of reaction can be calculated from the familiar equation

$$\begin{aligned}
\Delta G_{CMA} &= \Delta G^{\circ}_{CMA} + RTlnQ \\
&= \Delta G^{\circ}_{CMA} + RTln\left(\frac{[CMA]}{[C][M][A]}\right) \\
&= -17.9 + RTln\left(\frac{10^{-6}}{10^{-18}}\right) \\
&= -1.53\,kcal/mol
\end{aligned} \tag{9}$$

At this concentration, the ternary complex would be favored, but only modestly so. This quantity can be thought of as a free energy of ternary complex formation at a new standard state of one micromolar reactants and products. Although this standard state is unconventional, it is a certainly closer to cellular concentrations than the typical one molar standard state.

The concentration at which CSL is half-saturated with MAML and ANK at equilibrium can be calculated using equation 9. At this concentration, $\Delta G = 0$. From equation 9,

[4] For heterodimer formation, a free energy of -17.9 kcal/mol would result in saturation binding at micromolar concentrations in which heat peaks would drop abruptly from full amplitude to zero in a single injection.

$$0 = \Delta G^{\circ}_{CMA} + RTlnQ_{1/2} \tag{10}$$

where $Q_{1/2}$ gives the equilibrium concentration where $[CMA] = [C]$. Rearranging gives

$$\Delta G^{\circ}_{CMA} = -RTlnQ_{1/2} \tag{11}$$

Assuming equal total concentrations (i.e., $[C]_t = [M]_t = [A]_t$), $Q_{1/2}$ can be expressed as

$$\begin{aligned} Q_{1/2} &= \left(\frac{[CMA]}{[C][M][A]}\right)_{1/2} \\ &= \left(\frac{X}{X^3}\right)_{1/2} \\ &= \left(\frac{1}{X^2}\right)_{1/2} \end{aligned} \tag{12}$$

where X is the molar concentration that brings about half-saturation. Combining equations 12 and 11 gives

$$\Delta G^{\circ}_{CMA} = -17.9\, kcal/mol = +2RTlnX \tag{13}$$

Rearranging gives an free equilibrium concentration for half-saturation (X) of 275 nM, corresponding to total concentrations of $[C]_t = [M]_t = [A]_t = 550\, nM$. Thus, at half-micromolar total protein concentrations, the CMA ternary complex is half-formed. Below this concentration, the CSL:MAML:ANK ternary complex should be predominantly dissociated. Though the concentrations of CSL and MAML in the nucleus are not well known, recent work using Notch2 suggests nuclear concentrations of 2 nM [32]. Therefore it seems unlikely that the concentrations of NICD, CSL, and MAML would exceed 550 nM, and in the absence of bivalence, the CSL:MAML:ANK ternary complex would not be expected to assemble to high levels.

2.2 Analysis of bivalency in terms of effective concentration

Here we will analyze bivalency by comparing equilibrium constants. Because the dimensions of equilibrium constants are powers of molarity, this analysis provides a concentration-based view of bivalency, and justifies interpreting K_φ (the equilibrium constant associated with $\Delta G^{\circ}_{\varphi}$) as an effective concentration. To connect K_φ with effective concentration, it is helpful to relate K_φ to the two reactions that define it, namely K_{cis} (Table 1, reaction 8) and K_{CMA} (Table 1, reaction 6). Writing the standard state free energies from equation 6 in terms of equilibrium constants,

$$-RTlnK_\varphi = -RTlnK_{cis} + RTlnK_{CMA} \tag{14}$$

Rearranging gives K_φ as a ratio of binding constants for binding of ANK and MAML to CSL *in cis* and *in trans*:

$$K_\varphi = \frac{K_{cis}}{K_{CMA}} \tag{15}$$

Because K_{cis} and K_{CMA} have units of M^{-1} and M^{-2}, K_φ has units of M (that is, K_φ is a concentration). Using the value of ΔG°_φ fit in Figure 8, the value of K_φ is $20\mu M$. This value is rather low, an observation that is closely related to the rather large positive value of ΔG°_φ.

To demonstrate the relationship between K_φ and effective concentration, we can compare equations that give the fraction of CSL bound with ANK (and its obligate binding partner MAML) *in cis* and with ANK *in trans* ($\langle f_b^{cis}\rangle$ and $\langle f_b^{CMA}\rangle$). The fraction of CSL bound *in cis* with ANK is

$$\begin{aligned}\langle f_b^{cis}\rangle &= \frac{[CMA]}{[RC(A)]+[CMA]} \\ &= \frac{[CMA]/[RC(A)]}{1+[CMA]/[RC(A)]} \\ &= \frac{K_{cis}[M]}{1+K_{cis}[M]} \\ &= \frac{K_{CMA}K_\varphi[M]}{1+K_{CMA}K_\varphi[M]}\end{aligned} \tag{16}$$

As would be expected for a bimolecular reaction, $\langle f_b^{cis}\rangle$ is a simple rectangular hyperbola that depends on ligand concentration (here, MAML).

The fraction of CSL bound with ANK *in trans* is

$$\begin{aligned}\langle f_b^{CMA}\rangle &= \frac{[CMA]}{[C]+[CMA]} \\ &= \frac{[CMA]/[C]}{1+[CMA]/[C]} \\ &= \frac{K_{CMA}[A][M]}{1+K_{CMA}[A][M]}\end{aligned} \tag{17}$$

Although $\langle f_b^{CMA}\rangle$ becomes sigmoidal when both $[M]$ and $[A]$ are increased, it is a rectangular hyperbola in either $[M]$ or $[A]$ when the other is held constant[5]. This is shown in Figure 9, where ANK is titrated at constant MAML concentrations (solid curves). The ANK concentration that brings about half-saturation decreases with increasing MAML concentration, reflecting an apparent increase in ANK affinity. Indeed, at a fixed MAML concentration, the product $K_{CMA}[MAML]$ in equation 17 can be viewed as an apparent equilibrium constant that increases with MAML concentration. This apparent increase in binding affinity with increasing MAML concentration is the basis for the increased steepness of the integrated heat peaks in Figure 6[6].

In contrast, CSL saturation by ANK *in cis* does not depend on ANK concentration (equation 16). At a given MAML concentration, $\langle f_b^{cis}\rangle$ is constant (see the dashed lines in Figure 9), although it increases with MAML concentration in the same way as does $\langle f_b^{trans}\rangle$. The difference in the ANK dependence of $\langle f_b^{cis}\rangle$ and $\langle f_b^{CMA}\rangle$ results in a single intersection point between the two curves. Although the saturation value at this intersection point depends on MAML concentration, the ANK concentration at which these two curves

[5]Note that for this analysis, concentrations (i.e., $[M]$ and $[A]$) are free (rather than total) concentrations

[6]Though free MAML concentrations are not constant in actual ITC experiments

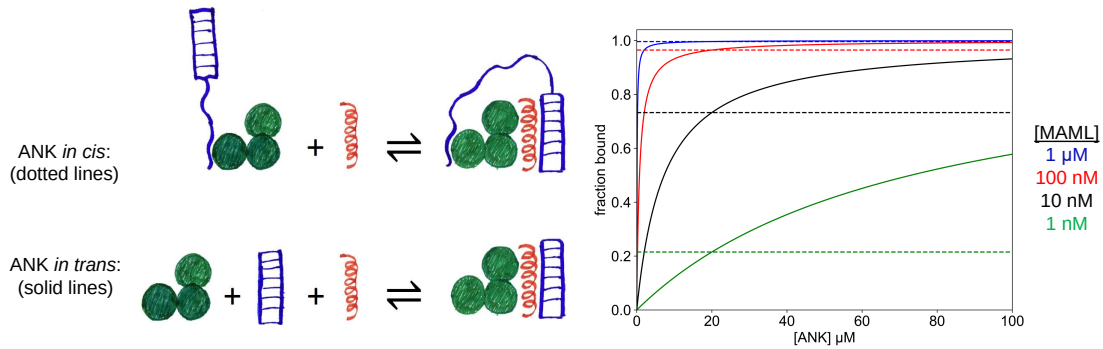

Figure 9: The fraction of ANK bound to CSL *in cis* and *in trans* at constant [MAML] concentrations. When ANK binds *in trans* at constant [MAML] (solid hyperbolas), it does so with an apparent binding constant of $K_{CMA}[MAML]$. When ANK binds *in cis* (dashed flat lines), a constant level of saturation is obtained, because the concentration of ANK is constant. The concentration of ANK where $\langle f_b^{cis} \rangle$ and $\langle f_b^{CMA} \rangle$ intersect is the effective concentration of ANK when tethered to CSL ($20\,\mu M$). Since $\langle f_b^{cis} \rangle$ and $\langle f_b^{CMA} \rangle$ both increase with [MAML], the effective concentration (the intersection point) remains constant.

intersect (which we will refer to as $[A]^*$) does not.

The significance of the intersection point between $\langle f_b^{cis} \rangle$ and $\langle f_b^{CMA} \rangle$ can be appreciated by comparing the expressions for these two quantities at the intersection point. At $[A] = [A]^*$, $\langle f_b^{cis} \rangle = \langle f_b^{CMA} \rangle$. Thus, from equations 16 and 17,

$$\frac{K_{CMA}K_{\varphi}[M]}{1 + K_{CMA}K_{\varphi}[M]} = \frac{K_{CMA}[A]^*[M]}{1 + K_{CMA}[A]^*[M]} \tag{18}$$

The only difference between the left- and right-hand sides of equation 18 (assuming MAML is at the same concentration on the left and right sides) is that K_{φ} on the left is replaced with $[A]^*$ on the right. Thus, to maintain the equality,

$$K_{\varphi} = [A]^* \equiv C_{eff} \tag{19}$$

In words, K_{φ} is the concentration of ANK that would be required to bring about the same saturation with ANK binding CSL *in trans* as is obtained with ANK binding CSL *in cis*. Alternatively, K_{φ} is the concentration of ANK when tethered by RAM bound to CSL, which is the definition of C_{eff}, the effective concentration. Thus, $K_{\varphi} = C_{eff}$.

2.3 The free energy of bivalent coupling at a dilute standard state

As alluded to in the results, the positive value of $\Delta G^{\circ}_{\varphi}$ is a result of the difference in stoichiometry of reactions 6 and 8 (from Table 1), and the use of a one molar standard state. Here we will explore how $\Delta G^{\circ}_{\varphi}$ changes when a more dilute (and more physiological) standard state is chosen. In general, a new standard state reaction free energy can be obtained using the equation

$$\Delta G^{new} = \Delta G^{\circ} + RT \ln Q^{new} \tag{20}$$

where ΔG^{new} is the reaction free energy at a new standard state, ΔG° is the reaction free energy at the 1 M standard state, and Q^{new} is the reaction quotient in which all concentrations are simultaneously changed to the new standard state concentration.

For simplicity we will choose a new standard state such that the concentrations of all reactants and products are the same. For the trans reaction,

$$[CMA]^{new} = [CSL]^{new} = [MAML]^{new} = [ANK]^{new} \equiv [i]^{new} \tag{21}$$

For the bivalent coupling,

$$[\varphi]^{new} \equiv [i]^{new} \tag{22}$$

These new standard state concentrations can be inserted into the Q^{new} term of equation 20 to generate free energies for the trans reaction and for bivalent coupling:

$$\begin{aligned} \Delta G^{new}_{CMA} &= \Delta G^{\circ}_{CMA} + RT \ln \frac{[CMA]^{new}}{[C]^{new}[M]^{new}[A]^{new}} \\ &= \Delta G^{\circ}_{CMA} + RT \ln \frac{[i]^{new}}{([i]^{new})^3} \\ &= \Delta G^{\circ}_{CMA} - 2RT \ln [i]^{new} \end{aligned} \tag{23}$$

$$\begin{aligned} \Delta G^{new}_{\varphi} &= \Delta G^{\circ}_{\varphi} + RT \ln [\varphi]^{new} \\ &= \Delta G^{\circ}_{\varphi} + RT \ln [i]^{new} \end{aligned} \tag{24}$$

Following from equations 24 and 23, the free energy of the cis reaction at a new standard state can be calculated using equation 6,

$$\Delta G^{new}_{cis} = \Delta G^{new}_{CMA} + \Delta G^{new}_{\varphi} \tag{25}$$

The standard state free energies in equation 25 are plotted as a function of standard state concentration (all reactants and products) in Figure 10. Because ΔG^{new}_{CMA} and ΔG^{new}_{cis} describe association reactions, they increase linearly with decreasing standard state concentration. However, they increase with different slopes due to their different stoichiometries, intersecting at the effective concentration ($20\mu M$). Because ΔG^{new}_{φ} is the difference between ΔG^{new}_{cis} and ΔG^{new}_{CMA} (equation 25), their difference in slope results in a decrease in ΔG^{new}_{φ} with decreasing standard state concentration, falling to zero at C_{eff}. Below C_{eff}, ΔG^{new}_{φ} is negative, indicating that the cis reaction (reaction 8, Table 1) is more favorable than the trans reaction (reaction 6, Table 1).

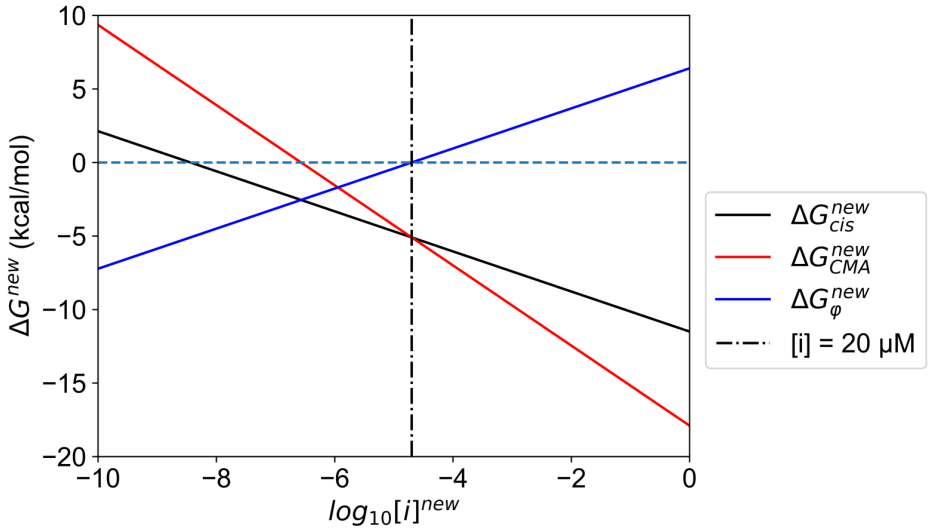

Figure 10: Dependence of free energies of ternary complex formation on standard state concentrations. ΔG^{new}_{cis}, ΔG^{new}_{CMA} and ΔG^{new}_{φ} are calculated as a function of standard state concentration [i] using equations 24 - 25. Because ΔG^{new}_{cis} and ΔG^{new}_{CMA} describe bimolecular and trimolecular association respectively, they have different slopes and therefore intersect, intersecting when the standard state is equal to C_{eff} (the vertical dash-dotted line). Below C_{eff}, more ternary complex is formed *in cis* than *in trans*, corresponding to a negative ΔG^{new}_{φ}.

2.4 Bivalency as a mechanism to couple RAM and ANK binding to CSL

Using the experimentally determined values of ΔG°_{CR}, ΔG°_{CMA}, $\Delta G^{\circ}_{\varphi}$ (Tables 2 and 3), we can determine the populations of partly and fully ligated species as a function of protein concentrations using binding polynomials for CSL. This approach provides a means to evaluate how the linkage of RAM and ANK binding to CSL *in cis* promotes bivalent ternary complex formation (CMRA), where both RAM and ANK are bound, over singly bound (CR(A), (R)CMA) ligation states.

Figure 11 shows the populations of different ligation states of CSL at different MAML concentrations when RAMANK is titrated. At high MAML concentration (Figure 11 A), CSL converts from completely unbound to the bivalent CMRA complex where both RAM and ANK are bound to their sites on CSL. The midpoint for this transition is 74 pM RAMANK. Populations of singly-ligated species (CR(A) and (R)CMA) are suppressed at all RAMANK concentrations. At high RAMANK concentrations, the bivalent CMRA complex shifts to the 2:1:1 RAMANK:CSL:MAML complex (R(A)CM(R)A, red curves, Figure 11). The RAMANK concentration at which the bivalent CMRA and tetrameric R(A)CM(R)A complexes have equal populations (the point at which the purple and red curves cross, Figure 11) is equal to the effective concentration C_{eff} (20 μM) regardless of the MAML concentration.

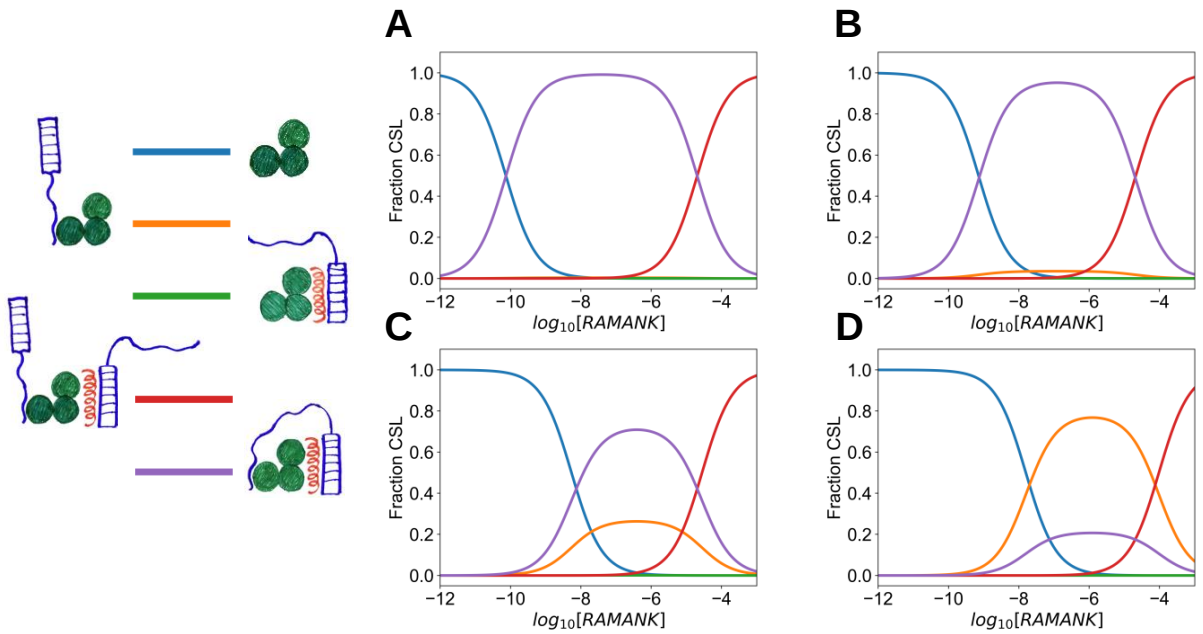

Figure 11: Populations of ligation states of CSL as a function of free (unbound) RAMANK and MAML concentration. The four panels show RAMANK titrations of CSL, MAML concentrations of (A) $1\mu M$, (B) 100 nM, (C) 10 nM, and (D) 1 nM. Curves correspond to different ligation states of CSL (see legend), calculated using the binding polynomial (equation 48, Appendix 2) and values of $\Delta G^{\circ}_{CR(A)}$, ΔG°_{CMA}, and $\Delta G^{\circ}_{\varphi}$ from Tables 2 and 3.

As the concentration of MAML is decreased, the midpoint for conversion from C to CMRA shifts to higher RAMANK concentrations (Figure 11 B,C,D). The magnitude of this shift is inversely proportional to the change in MAML concentration: decreasing MAML by one order of magnitude ($1\ \mu M$ to $100\ nM$) increases the midpoint from $74\ pM$ to $740\ pM$. Another order of magnitude decrease ($[MAML] = 10\ nM$) increases the midpoint to $7.4\ nM$, and a further decrease ($[MAML] = 1\ nM$) increases the midpoint to $74\,nM$. Although the monovalently-ligated species are suppressed at high MAML concentrations, as MAML concentration decreases to the 1-10 nM range, the species of CSL bound with RAM but with ANK dissociated (CR(A), orange curve, Figure 11) is formed at appreciable concentrations.

In addition to comparing the different ligation states of CSL in complex with RAMANK, the binding polynomial (Appendix 2) can be used to determine the extent to which bivalency increases RAM and ANK binding, by comparing the occupancy of RAM and ANK at their CSL binding sites when on a single polypeptide (capable of binding to CSL *in cis*) to occupancies when RAM and ANK are on two separate polypeptides (only capable of binding to CSL *in trans*) (Figure 12). When RAM and ANK are on the same polypeptide, occupancy at their respective sites is half-saturated at 74 pM (at $1\mu M$ MAML), whereas titration with separate RAM and ANK polypeptides does not half-saturate until 20 and 76 nM (Figure 12 A,B). Thus, bivalency increases occupancy at both sites by about three orders of magnitude.

Moreover, whereas the ternary bivalent CMRA species is the dominant ligation state when RAM and

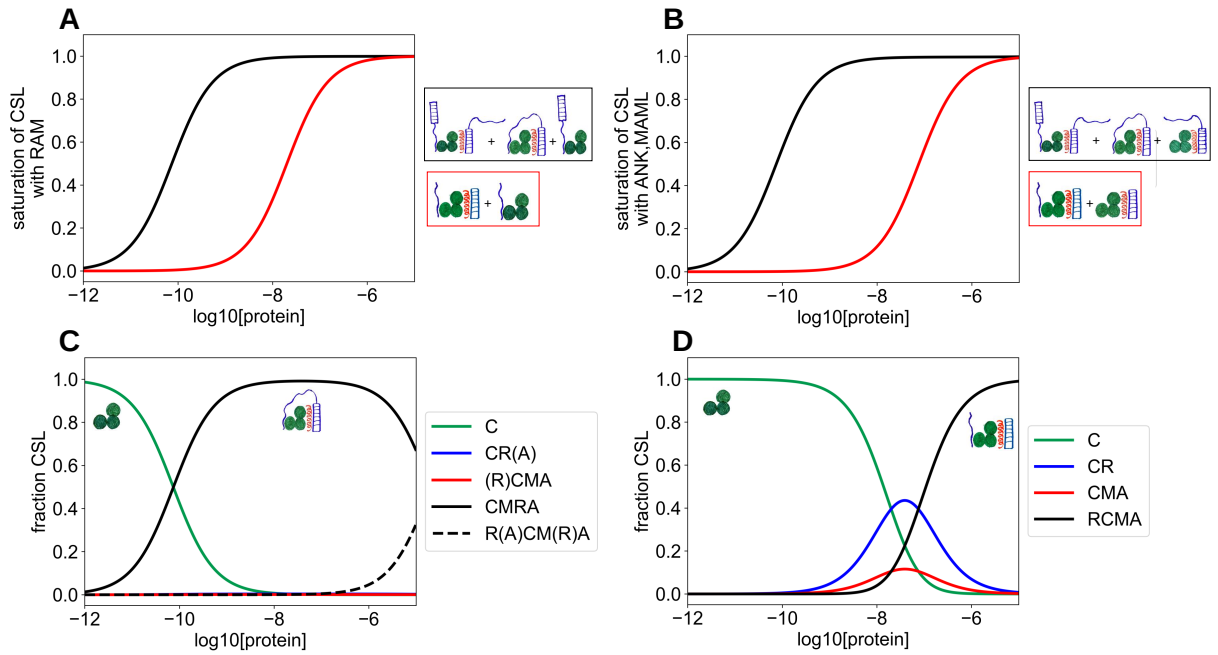

Figure 12: Comparison of CSL saturation with RAMANK (one polypeptide) to saturation with RAM and ANK (two separate polypeptides) at equal concentrations. (A) Saturation of CSL with RAM when RAM and ANK are on the same polypeptide (black), and when RAM and ANK are at the same concentrations but on separate polypeptides (red). (B) Saturation of CSL with ANK and MAML, when RAM and ANK are on the same polypeptide (black), and when RAM and ANK are on separate polypeptides at the same concentrations (red). Saturation in (A) and (B) includes all species in which RAM (A) and ANK + MAML (B) are directly bound to their sites on CSL. (C) shows ligation states of CSL with RAMANK (one polypeptide), and (D) shows ligation states of CSL with RAM and ANK (two polypeptides). In all four plots, MAML is at a concentration of $1\mu M$ and all concentrations are free (rather than total).

ANK are on the same polypeptide (Figures 11, 12C), half-ligated states populate significantly when RAM and ANK are two separate polypeptides (Figure 12D). The doubly ligated RCMA state (black curve, Figure 12D) is not half-saturated until 110 nM RAM and ANK. This analysis shows that the covalent linkage between RAM and ANK enhances CSL saturation by three orders of magnitude, combining two moderate affinity interactions to facilitate saturation at sub-nanomolar concentrations.

3 Methods

3.1 Expression and purification of CSL, RAM, RAMANK, and ANK

Protein samples of CSL, RAM, RAMANK, and ANK were expressed and purified as in [29] and [21], using modified pMAL-c2x expression vectors with N-terminal His_{12} tags and MBP solubility tags. Briefly, expression vectors were transformed into *E. coli* strain BL21(DE3) and grown with Ampicillin at 37°C while shaking at 200rpm to an O.D.600 between 0.6-0.8. Expression was induced by adding IPTG to 1mM and shaking at 200rpm and 20°C for 12-18 hours. Cells were pelleted by centrifugation at 4,424×g and stored

at -80°C. For purification, cell pellets were thawed to 20°C and resuspended in 25mM Tris, 50mM NaCl, 0.5mM tris(2-carboxyethyl)phosphine (TCEP), pH8 (lysis buffer) and one c0mplete protease inhibitor tablet (Roche catalog no. 11836170001) per 100 mL lysate. Resuspended cells were sonicated on ice and were centrifuged at 30,966×g for 40 minutes at 4°C. The cleared supernatant was brought to 2mM $MgCl_2$ and treated with DNaseI and benzonase at 20°C for 1 hour. The sample was brought to 500mM NaCl (now in equilibration buffer; 25mM Tris, 500mM NaCl, 0.5mM TCEP, pH8) and loaded onto a Ni-NTA gravity column at 4°C. The column was washed with equilibration buffer containing 100 mM imidazole, and protein was eluted using equilibration buffer containing 750 mM imidazole. Eluted protein was dialyzed into 25 mM Na Phos, 150 mM NaCl, 0.5 mM TCEP pH7 (ion exchange buffer A) overnight at 4°C in the presence of 2 mg TEV protease. Cleaved sample was passed over a Ni-NTA gravity column at 4°C to remove any uncleaved protein. The Ni-NTA column was washed with ion exchange buffer A containing 10mM imidazole. The flow-through and wash were collected, filtered, and purified using either a HiTrapQ HF anion exchange column or a HiTrapSP HF cation exchange column (Cytiva) by eluting with a linear gradient of 1 mM to 1 M NaCl in 25 mM Na Phos, 0.5 mM TCEP, pH7. Fractions containing pure protein, as judged by SDS PAGE, were combined and dialyzed at 4°C in 25 mM Na Phos, 150 mM NaCl, 0.5 mM TCEP pH7.

3.2 Expression and purification of MAML

Human MAML1 (residues 8-76) with a C-terminal tryptophan for concentration measurement was expressed and purified as in [26] using a pET expression vector with an N-terminal His_6 tag and a SUMO solubility tag. Briefly, the expression vector was transformed into *E. coli* strain BL21(DE3) and grown with Kanamycin at 37°C while shaking at 200rpm to an O.D.600 of 0.8. Expression was induced as described above for CSL. Cells were pelleted by centrifugation at 5,000×g and resuspended, lysed, and pelleted as described above for CSL. His-SUMO-MAML1-W localizes to the lysate pellet, which was washed twice in 100 mM Tris pH 7.4, 5 mM EDTA, 1 M urea, 0.5 mM TCEP, 1% Triton X-100 followed by a wash in 100 mM Tris pH 7.4 and 0.5 mM TCEP. Pellets were re-suspended using a Dounce homogenizer and re-pelleted by centrifugation at 15,000×g for 25 minutes. The washed pellet was resuspended in 8 M urea, 25 mM Tris pH 8.0, 250 mM NaCl, 0.5 mM TCEP (binding buffer) and batch bound to Ni-NTA resin overnight with rotation at 4°C. The resin was loaded onto a gravity column and washed with binding buffer to remove unbound protein. Protein was refolded while bound to the resin by washing with 25 mM Tris pH 8.0, 250 mM NaCl, 0.5 mM TCEP (refold buffer). His-SUMO-MAML1W was eluted from the resin using refold buffer containing 300 mM imidazole, and the sample was brought to 100 mM EDTA. SUMO protease Ulp1 was added to the His-SUMO-MAML1W, and sample was dialyzed 8 hours at 4°C in 50 mM Tris pH 8.0, 150 mM NaCl, 0.5 mM TCEP, 5% glycerol followed by dialysis overnight at 4°C in 25 mM Na Phos pH 8.0, 50 mM NaCl, 0.5 mM TCEP. Cleaved sample was centrifuged at 15,000×g for 30 minutes to remove precipitated aggregates. Sample was purified using a HiTrapSP HF column (Cytiva) and eluted using a linear gradient from 50 mM to 1 M NaCl in 25 mM Na Phos pH 8.0, 0.5 mM TCEP. Fractions containing pure protein, as determined by SDS PAGE, were combined and dialyzed at 4°C in 25 mM Na Phos, 150 mM NaCl, 0.5 mM TCEP pH7.

3.3 Isothermal Titration Calorimetry

Purified protein samples were dialyzed in 25 mM Na Phos, 150 mM NaCl, 0.5 mM TCEP, pH7 (dialysis buffer) at 4°C overnight. Proteins were $0.2\mu m$ filtered using 13 mm diameter PVDF filters (Thermo Fisher part no. CH2213-PV). Protein concentrations were determined from their ultraviolet absorbance and their calculated extinction coefficients [12]. NaCl was added to dialysis buffer, filtered, and used to bring experimental samples to 200 mM NaCl. Samples were left to equilibrate for twenty minutes before loading into a MicroCal VP-ITC. Experiments were performed at 25°C unless otherwise described, injection volumes were $8\mu L$, and injection intervals were 5 minutes. Initial concentrations of proteins were as described throughout the paper, but typically $20\mu M$ protein was loaded in the syringe and $2\mu M$ of CSL was loaded in the calorimeter cell (with or without another protein in the cell in excess of $2\mu M$). Raw thermogram injection peaks were baseline-corrected and integrated using NITPIC [17] and fit using the equations described in Appendix 1 or 3. Fitted parameters were from global fits of three experiments, and uncertainties are standard errors from the covariance matrix.

4 Appendix 1. Solution of the cubic equation for CMA, and inclusion of the effects of dilution due to titration

As described above, when the mass-action expression for the ternary equilibrium constant is expressed in terms of total (rather than free) concentrations of CSL, MAML, and ANK (equation 4), the resulting expression is cubic in the concentration of the ternary complex. This is clearly revealed by rearranging equation 4 and collecting like terms:

$$\begin{aligned} 0 &= [CMA]^3 - ([C]_t + [M]_t + [A]_t)[CMA]^2 + ([C]_t[M]_t + [M]_t[A]_t + [C]_t[A]_t + 1/K_{CMA})[CMA] - [C]_t[M]_t[A]_t \\ &= a[CMA]^3 + b[CMA]^2 + c[CMA] + d \end{aligned} \tag{26}$$

where

$$a = 1 \tag{27}$$

$$b = -([C]_t + [M]_t + [A]_t) \tag{28}$$

$$c = [C]_t[M]_t + [M]_t[A]_t + [C]_t[A]_t + 1/K_{CMA} \tag{29}$$

$$d = -[C]_t[M]_t[A]_t \tag{30}$$

Although the three roots of equation 26 can be expressed analytically in terms of square and cube roots, these roots contain complex numbers and cannot be used for curve fitting. An alternative approach, which generates real roots, involves rearranging the cubic equation to eliminate the quadratic term. The roots of this rearranged (or "depressed") cubic can be expressed using trigonometric functions rather than radicals. Obtaining a depressed cubic equation is achieved by a substitution of variables from $[CMA]$ to x:

$$[CMA] = x - \frac{b}{3a} \tag{31}$$

where a and b are as defined above. Substituting [CMA] in equation 26 with the right hand side of equation 31 and rearranging gives

$$x^3 + \left(\frac{3ac–b^2}{3a^2}\right)x + \frac{3b^3–9abc–27a^2d}{27a^3} = 0 \tag{32}$$

This is of the form

$$x^3 + px + q = 0 \tag{33}$$

where

$$p = \frac{3ac–b^2}{3a^2} \tag{34}$$

$$q = \frac{3b^3–9abc–27a^2d}{27a^3} \tag{35}$$

The three roots of the depressed cubic (equation 33) are given by the trigonometric formula

$$\begin{aligned} x_k &= 2\sqrt{\frac{-p}{3}}\cos\left[\frac{1}{3}\arccos\left(\frac{3q}{2p}\sqrt{\frac{-3}{p}}\right) - \frac{2\pi k}{3}\right] \\ &= 2\sqrt{\frac{-\frac{3ac–b^2}{3a^2}}{3}}\cos\left[\frac{1}{3}\arccos\left(\frac{3\frac{3b^3–9abc–27a^2d}{27a^3}}{2\frac{3ac–b^2}{3a^2}}\sqrt{\frac{-3}{\frac{3ac–b^2}{3a^2}}}\right) - \frac{2\pi k}{3}\right] \end{aligned} \tag{36}$$

where $k = 0$, 1, or 2; for the ITC titrations here, the third root ($k = 2$) corresponds to positive values of [CMA]. Substituting $k = 2$ and $a = 1$ into equation 36 gives

$$\begin{aligned} x_2 &= 2\sqrt{\frac{-\frac{3c–b^2}{3}}{3}}\cos\left[\frac{1}{3}\arccos\left(\frac{3\frac{3b^3–9bc–27d}{27}}{2\frac{3c–b^2}{3}}\sqrt{\frac{-3}{\frac{3c–b^2}{3}}}\right) - \frac{4\pi}{3}\right] \\ &= \frac{2}{3}\sqrt{b^2 - 3c}\cos\left[\frac{1}{3}\arccos\left(\frac{b^3–3bc–9d}{6c–2b^2}\sqrt{\frac{9}{b^2 - 3c}}\right) - \frac{4\pi}{3}\right] \end{aligned} \tag{37}$$

An expression for $[CMA]$ can be obtained from x_2 by substituting a rearranged version of equation 31, i.e.

$$x_2 = [CMA] + \frac{b}{3a} \tag{38}$$

The resulting expression gives [CMA] as a function of the total concentrations $[C]_t$, $[M]_t$, and $[A]_t$. As described in footnote 2, although total concentrations are uniquely determined from the known starting concentrations in the cell ($[C]_0$, $[A]_0$) and the syringe ($[M]_0$), they need to be calculated after each injection

to account for dilution and displacement effects. For proteins in the cell, each injection displaces some of the sample; the fraction of the sample displaced is equal to $(1 - \frac{V_i}{V_c})$ where V_i and V_c are the volume of the injection and cell, respectively. Cell proteins are diluted by this factor after each injection; thus, after injection j, the total protein concentrations are given by

$$[C]_t = [C]_0 \left(1 - \frac{V_i}{V_c}\right)^j \tag{39}$$

$$[A]_t = [A]_0 \left(1 - \frac{V_i}{V_c}\right)^j \tag{40}$$

For the protein in the syringe (MAML in Figure 6), the first injection adds an amount of protein that is diluted by the ratio of the cell volume to the syringe volume, i.e.,

$$\begin{aligned} [M]_t &= [M]_0 \frac{V_i}{V_c} \\ &= [M]_0 \left[1 - \left(1 - \frac{V_i}{V_c}\right)\right] \end{aligned} \tag{41}$$

The rearrangement in the second line puts the $[M]_t$ expression in the same form as expressions for subsequent injections. The second injection dilutes the MAML provided from the first injection (now in the cell) as in equations 39 and 40, and also adds another dilution from the syringe. Thus,

$$\begin{aligned} [M]_t &= [M]_0 \frac{V_i}{V_c} \left(1 - \frac{V_i}{V_c}\right) + [M]_0 \frac{V_i}{V_c} \\ &= [M]_0 \left[2\frac{V_i}{V_c} - \left(\frac{V_i}{V_c}\right)^2\right] \\ &= [M]_0 \left[1 - \left(1 - \frac{V_i}{V_c}\right)^2\right] \end{aligned} \tag{42}$$

The third injection acts the same as the second, diluting MAML from the second injection and adding another dilution:

$$\begin{aligned} [M]_t &= [M]_0 \left[1 - \left(1 - \frac{V_i}{V_c}\right)^2\right] \left(1 - \frac{V_i}{V_c}\right) + [M]_0 \frac{V_i}{V_c} \\ &= [M]_0 \left[1 - \frac{V_i}{V_c} - \left(1 - \frac{V_i}{V_c}\right)^3\right] + [M]_0 \frac{V_i}{V_c} \\ &= [M]_0 \left[1 - \left(1 - \frac{V_i}{V_c}\right)^3\right] \end{aligned} \tag{43}$$

Comparing equations 41, 42, and 43 reveals a general formula for the total concentration of the syringe

protein after the jth injection:

$$[M]_t = [M]_0 \left[1 - \left(1 - \frac{V_i}{V_c} \right)^j \right] \tag{44}$$

With these equations, an expression for the concentration of the ternary complex ($[CMA]$) can be generated with the following steps:

1. Substitute expressions for $[C]_t$, $[M]_t$, and $[A]_t$ (equations 39, 44, and 40) into the equations for the coefficients to the cubic equation for $[CMA]$ (a, b, c, and d, equations 27 - 30).
2. Substitute the modified cubic coefficients from step 1 into the equation for x_2 (equation 37).
3. Substitute the modified expression for x_2 from step 2 into the change-of-variable equation for $[CMA]$ (equation 31).
4. Substitute the modified expression for $[CMA]$ from step 3 into the heat equation (equation 2).

Although the resulting fitting equation (from step 4) is too long to fit on a page, it can easily be generated using the sympy module of python, and can be converted using the sympy.lambdify command to generate an equation that can be fit to ITC data (represented as a numpy array). Single ITC data sets are fit using the scipy.optimize.curvefit command. Multiple ITC data sets are globally fitted using the lmfit module. A jupyter notebook that generates this fitting function (along with sample data) is available on github.

5 Appendix 2. Binding polynomials for RAMANK and MAML binding to CSL *in cis* and *in trans*

Analysis of ligand binding often requires expressions for fractions of macromolecules in different states of assembly. One convenient expression to represent such fractions is the binding polynomial [35, 2]. The binding polynomial is composed of statistical weights that represent the concentrations of ligation states of a macromolecule relative to its unbound state. Replacing concentrations with equilibrium constants generates a polynomial in powers of ligand concentration (or concentrations when there is more than one ligand).

Here we present binding polynomials that describe the saturation state of CSL with various ligands (RAM, ANK, RAMANK, and MAML). In these polynomials, unbound CSL serves as the reference state for the various bound forms of CSL. These polynomials are useful for calculating populations of CSL in various ligation states (Figures 11 and 12) and for generating expressions for numerical analysis of binding data. When RAM and ANK are *in trans* in the presence of MAML, the CSL binding polynomial has four terms:

$$P_{trans} = \frac{[C]}{[C]} + \frac{[CR]}{[C]} + \frac{[CMA]}{[C]} + \frac{[RCMA]}{[C]} \tag{45}$$

Substituting concentration ratios with equilibrium constants gives

$$P_{trans} = 1 + \beta_{CR}[R] + \beta_{CMA}[M][A] + \beta_{CR}\beta_{CMA}[R][A][M] \tag{46}$$

When RAM and ANK are *in cis* in the presence of MAML, the CSL binding polynomial has five terms:

$$P_{cis} = \frac{[C]}{[C]} + \frac{[CR(A)]}{[C]} + \frac{[CM(R)A]}{[C]} + \frac{[CMRA]}{[C]} + \frac{[R(A)CM(R)A]}{[C]} \tag{47}$$

Substituting concentration ratios with equilibrium constants gives

$$P_{cis} = 1 + \beta_{CR(A)}[RA] + \beta_{CMA}[M][RA] + \beta_{CR(A)}\beta_{CMA}\varphi[RA][M] + \beta_{CR(A)}\beta_{CMA}[RA]^2[M] \tag{48}$$

The fraction of total macromolecule that forms a particular species can be calculated by dividing the statistical weight of the species by the binding polynomial. For example, the fraction of CSL in that is in the bivalent ternary complex (CMRA) is

$$f_{CMRA} = \frac{\beta_{CR(A)}\beta_{CMA}\varphi[RA][M]}{P_{cis}} \tag{49}$$

Likewise, the fraction of total CSL in the tetrameric complex R(A)CM(R)A is

$$f_{R(A)CM(R)A} = \frac{\beta_{CR(A)}\beta_{CMA}[RA]^2[M]}{P_{cis}} \tag{50}$$

6 Appendix 3. Numerical derivations for analysis of ITC data including the tetrameric R(A)CM(R)A complex

As described above, the fitted value of $\Delta G^{\circ}_{\varphi}$ obtained from the titration of MAML into mixtures of CSL saturated with RAMANK indicates that at high concentrations of RAMANK, a non-neglibile amount of heterotetramer complex should form with two RAMANK, one CSL, and one MAML (R(A)CM(R)A, Figure 2), and should be included in fits of titrations of prebound CSL-RAMANK complexes with MAML. Modifying the equation for heats of injection (equation 2) to include this additional species gives

$$\begin{aligned} q_i = {} & \Delta H_{CMA}\big(n_i - n_{i-1}\big)_{CMA} + \Delta H_{tet}\big(n_i - n_{i-1}\big)_{tet} \\ & + \Delta H_{CR(A)}\big(n_i - n_{i-1}\big)_{CR(A)} + \Delta H_{CMRA}\big(n_i - n_{i-1}\big)_{CMRA} \end{aligned} \tag{51}$$

where the tetrameric species R(A)CM(R)A is abbreviated "tet". The terms in parenthesis are the number of moles of each species in the cell at injection i. Substituting the mole number for each species with concentration gives

$$\begin{aligned} q_i = V_{cell}\Big\{ & \Delta H_{CMA}\big([CMA]_i - [CMA]_{i-1}\big) + \Delta H_{tet}\big([tet]_i - [tet]_{i-1}\big) \\ & + \Delta H_{CR(A)}\big([CR(A)]_i - [CR(A)]_{i-1}\big) + \Delta H_{CMRA}\big([CMRA]_i - [CMRA]_{i-1}\big)\Big\} \end{aligned} \tag{52}$$

where V_{cell} is the volume of the calorimetry cell. Replacing molar concentrations of each species with species fractions gives

$$q_i = V_{cell}[C]_t\Big\{\Delta H_{CMA}\big(f_{CMA,i} - f_{CMA,i-1}\big) + \Delta H_{tet}\big(f_{tet,i} - f_{tet,i-1}\big) + \Delta H_{CR(A)}\big(f_{CR(A),i} - f_{CR(A),i-1}\big) + \Delta H_{CMRA}\big(f_{CMRA,i} - f_{CMRA,i-1}\big)\Big\} \tag{53}$$

The species fractions can be calculated directly from the binding polynomial (Appendix 2), given a set of binding constants and unbound MAML and RAMANK concentrations. Unfortunately, calculating unbound concentrations from known total concentrations and equilibrium constants leads to an equation that is quartic in $[tet]$ (and cubic in $[CMA]$). Rather than attempting to solve this equation analytically, we have used a numerical method to determine the concentrations of species needed to fit ITC titrations of MAML into CSL and RAMANK. This approach follows that of Vega *et al.* [33].

In the approach of Vega et al., the binding polynomial is used to generate expressions for concentrations of unbound species species in terms of total concentrations, and unbound concentrations are determined using a numerical root-finding algorithm. For titration of CSL and RAMANK with MAML, there are three such equations. For CSL,

$$[C] = f_C[C]_t = \frac{1}{P_{cis}}[C]_t \tag{54}$$

where f_C is the fraction of total CSL in the free state. In the expression on the right-hand-side, the one in the numerator is the statistical weight of free CSL, which is the reference state in the polynomial (see Appendix 2, equation 47).

An analogous expression for free MAML is derived from a conservation expression which states the total MAML concentration is equal to the sum of all species that include MAML,

$$\begin{aligned}
[M] &= [M]_t - [CMA] - [CMRA] - [tet] && (55)\\
&= [M]_t - f_{CMA}[C]_t - f_{CRMA}[C]_t - f_{tet}[C]_t && (56)\\
&= [M]_t - [C]_t\Big(f_{CMA} + f_{CRMA} + f_{tet}\Big) && (57)\\
&= [M]_t - [C]_t\left(\frac{\beta_{CMA}[M][RA]}{P_{cis}} + \frac{\beta_{CR(A)}\beta_{CMA}\varphi[RA][M]}{P_{cis}} + \frac{\beta_{CR(A)}\beta_{CMA}[RA]^2[M]}{P_{cis}}\right) && (58)\\
&= [M]_t - [C]_t\left(\frac{\beta_{CMA}[M][RA] + \beta_{CR(A)}\beta_{CMA}\varphi[RA][M] + \beta_{CR(A)}\beta_{CMA}[RA]^2[M]}{P_{cis}}\right) && (59)\\
&= [M]_t - [C]_t\frac{[M]}{P_{cis}}\left(\frac{\partial P_{cis}}{\partial [M]}\right) && (60)\\
&= [M]_t - [C][M]\left(\frac{\partial P_{cis}}{\partial [M]}\right) && (61)
\end{aligned}$$

The reason this equation has more terms than that for $[C]$ (equation 54) is that the binding polynomial P_{cis} is referenced to unbound CSL. The derivative in equations 60 and 61 provide a shorthand for the cluttered equations 58 and 64 [35, 2].

Likewise, the expression for free RAMANK is

$$
\begin{aligned}
[RA] &= [RA]_t - [CR(A)] - [CMRA] - 2[tet] && (62)\\
&= [RA]_t - f_{CR(A)}[C]_t - f_{CRMA}[C]_t - 2f_{tet}[C]_t && (63)\\
&= [RA]_t - [C]_t\left(\frac{\beta_{CR(A)}[RA] + \beta_{CR(A)}\beta_{CMA}\varphi[RA][M] + 2\beta_{CR(A)}\beta_{CMA}[RA]^2[M]}{P_{cis}}\right) && (64)\\
&= [RA]_t - [C]_t\frac{[RA]}{P_{cis}}\left(\frac{\partial P_{cis}}{\partial [RA]}\right) && (65)\\
&= [RA]_t - [C][RA]\left(\frac{\partial P_{cis}}{\partial [RA]}\right) && (66)
\end{aligned}
$$

The factor of two multiplying $[tet]$ accounts for the fact that there are two RAMANK molecules in the tetramer.

Rearranging the three expressions for unbound concentrations of CSL, MAML, and RAMANK (equations 54, 61, and 66) gives

$$P_{cis}[C] - [C]_t \equiv g_{C_t}([C],[M],[RA]) \tag{67}$$

$$[M] + [C][M]\left(\frac{\partial P_{cis}}{\partial [M]}\right) - [M]_t = 0 \equiv g_{M_t}([C],[M],[RA]) \tag{68}$$

$$[RA] + [C][RA]\left(\frac{\partial P_{cis}}{\partial [RA]}\right) - [RA]_t = 0 \equiv g_{RA_t}([C],[M],[RA]) \tag{69}$$

The g functions on the right-hand side is a shorthand to simplify the derivation below. Solving for $[C]$, $[M]$, and $[RA]$ is equivalent to simultaneously finding the roots of equations 67, 68, and 69 given total concentrations $[C]_t$, $[M]_t$, and $[RA]_t$. For a single-variable function $g(x)$, the root can be found iteratively using the Newton-Raphson method. Starting with an initial guess x_0 in the range of the true root x_t, a better approximation to the root is given by

$$x_1 = x_0 - \frac{g(x_0)}{\partial g(x_0)/\partial x} \tag{70}$$

This method is repeated iteratively for some number of steps k at which a convergence criterion is satisfied:

$$\left|\frac{x_k - x_{k-1}}{x_{k-1}}\right| < \epsilon \tag{71}$$

The same iterative approach can be used to simultaneously find the roots to equations 67, 68, and 69 where the initial guess x_0 is replaced with a vector of initial guesses of concentration:

$$\vec{X_0} = \begin{pmatrix} [C]_0 \\ [M]_0 \\ [RA]_0 \end{pmatrix} \tag{72}$$

The function g_x is replaced by a vector $\vec{G}$ composed of the three functions:

$$\vec{G} = \begin{pmatrix} g_{C_t}([C],[M],[RA]) \\ g_{M_t}([C],[M],[RA]) \\ g_{RA_t}([C],[M],[RA]) \end{pmatrix} \tag{73}$$

The derivative $\partial g/\partial x$ is replaced by the Jacobian matrix $J(\vec{G})$:

$$J(\vec{G}) = \begin{pmatrix} \frac{\partial g_{C_t}}{\partial [C]} & \frac{\partial g_{C_t}}{\partial [M]} & \frac{\partial g_{C_t}}{\partial [RA]} \\ \frac{\partial g_{M_t}}{\partial [C]} & \frac{\partial g_{M_t}}{\partial [M]} & \frac{\partial g_{M_t}}{\partial [RA]} \\ \frac{\partial g_{RA_t}}{\partial [C]} & \frac{\partial g_{RA_t}}{\partial [M]} & \frac{\partial g_{RA_t}}{\partial [RA]} \end{pmatrix} \tag{74}$$

With these substitutions, the Newton-Raphson algorithm becomes

$$\vec{X_1} = \vec{X_0} - J(\vec{G_0})^{-1} \times \vec{G_0} \tag{75}$$

where $J(\vec{G_0})^{-1}$ is the inverse of the Jacobian matrix evaluated at $\vec{X_0}$. Estimates of $[C]$, $[M]$, and $[RA]$ are iteratively updated using equation 75 taking the output of the previous iteration $\vec{X}_{i-1}$ as input:

$$\vec{X}_i = \vec{X}_{i-1} - J(\vec{G}_{i-1})^{-1} \times \vec{G}_{i-1} \tag{76}$$

Optimization is terminated when three convergence criteria are simultaneously satisfied:

$$\left| \frac{[C]_k - [C]_{k-1}|}{|[C]_{k-1}} \right| < \epsilon \tag{77}$$

$$\left| \frac{[M]_k - [M]_{k-1}}{[M]_{k-1}} \right| < \epsilon \tag{78}$$

$$\left| \frac{[RA]_k - [RA]_{k-1}}{[RA]_{k-1}} \right| < \epsilon \tag{79}$$

where ϵ is typically on the order of 10^{-6}.

To fit ITC data, total concentrations ($[C]_t$, $[M]_t$, and $[RA]_t$) are calculated for each injection using equations 39, 44, and 40 along with the starting cell and syringe concentrations ($[C]_0$, $[M]_0$, and $[RA]_0$). These total concentrations are used in Newton-Raphson to find unbound concentrations $[C]$, $[M]$, and $[RA]$ at each injection.

Combining these unbound concentrations with initial guesses for equilibrium constants[7], the binding polynomial is evaluated at each injection, giving the species fractions needed to calculate heats of injection using equation 53. Calculated heats are subtracted from experimentally determined values and are supplied

[7] Or with updated values during the fit.

to the nonlinear least squares module lmfit [25] to optimize fit parameters (binding constants, enthalpies, and the incompetent fraction of MAML). With this approach, Newton-Raphson is rerun at every injection point in each round of nonlinear least squares optimization using updated fit parameters. Fitting single titrations, convergence times for lmfit are on the order of 80 seconds.[8]. A jupyter notebook containing the code for numerical fitting, along with some sample ITC data, can be downloaded from Github.

References

[1] Jon C. Aster, Warren S. Pear, and Stephen C. Blacklow. The Varied Roles of Notch in Cancer. *Annual review of pathology*, 12:245, December 2016.

[2] Douglas Barrick. *Biomolecular Thermodynamics: From Theory to Application*. CRC Press, Boca Raton, 1 edition edition, September 2017.

[3] Angela Bertagna, Dima Toptygin, Ludwig Brand, and Doug Barrick. The effects of conformational heterogeneity on the binding of the Notch intracellular domain to effector proteins: a case of biologically tuned disorder. *Biochemical Society Transactions*, 36(Pt 2):157–166, April 2008.

[4] Cristina Del Bianco, Jon C. Aster, and Stephen C. Blacklow. Mutational and energetic studies of Notch1 transcription complexes. *Journal of molecular biology*, 376(1):131–140, February 2008.

[5] Eike-Benjamin Braune and Urban Lendahl. Notch – a goldilocks signaling pathway in disease and cancer therapy. *Discovery Medicine*, 21(115):189–196, March 2016.

[6] Sarah J. Bray. Notch signalling in context. *Nature Reviews Molecular Cell Biology*, 17(11):722–735, November 2016. Publisher: Nature Publishing Group.

[7] Sung Hee Choi, Thomas E. Wales, Yunsun Nam, Daniel J. O'Donovan, Piotr Sliz, John R. Engen, and Stephen C. Blacklow. Conformational Locking upon Cooperative Assembly of Notch Transcription Complexes. *Structure*, 20(2):340–349, February 2012. Publisher: Elsevier.

[8] Ashley N. Contreras, Zhenyu Yuan, and Rhett A. Kovall. Thermodynamic binding analysis of Notch transcription complexes from Drosophila melanogaster. *Protein Science: A Publication of the Protein Society*, 24(5):812–822, May 2015.

[9] John S. Dexter. The Analysis of a Case of Continuous Variation in Drosophila by a Study of Its Linkage Relations. *The American Naturalist*, 48(576):712–758, December 1914. Publisher: The University of Chicago Press.

[10] Robert Fraczkiewicz and Werner Braun. Exact and efficient analytical calculation of the accessible surface areas and their gradients for macromolecules. *Journal of Computational Chemistry*, 19(3):319–333, 1998. _eprint: https://onlinelibrary.wiley.com/doi/pdf/10.1002/%28SICI%291096-987X%28199802%2919%3A3%3C319%3A%3AAID-JCC6%3E3.0.CO%3B2-W.

[8] The slowest part of the numerical fitting procedure is calculating the Jacobian and its inverse, which only needs to be done once.

[11] David R. Friedmann, Jeffrey J. Wilson, and Rhett A. Kovall. RAM-induced Allostery Facilitates Assembly of a Notch Pathway Active Transcription Complex. *Journal of Biological Chemistry*, 283(21):14781–14791, May 2008.

[12] Elisabeth Gasteiger, Alexandre Gattiker, Christine Hoogland, Ivan Ivanyi, Ron D. Appel, and Amos Bairoch. ExPASy: the proteomics server for in-depth protein knowledge and analysis. *Nucleic Acids Research*, 31(13):3784–3788, July 2003.

[13] J. Gómez, V. J. Hilser, D. Xie, and E. Freire. The heat capacity of proteins. *Proteins*, 22(4):404–412, August 1995.

[14] S. Jarriault, C. Brou, F. Logeat, E. H. Schroeter, R. Kopan, and A. Israel. Signalling downstream of activated mammalian Notch. *Nature*, 377(6547):355–358, September 1995.

[15] Scott E. Johnson and Douglas Barrick. Dissecting and Circumventing the Requirement for RAM in CSL-Dependent Notch Signaling. *PLOS ONE*, 7(8):e39093, August 2012.

[16] Scott E. Johnson, M. Xenia G. Ilagan, Raphael Kopan, and Doug Barrick. Thermodynamic Analysis of the CSL·Notch Interaction: DISTRIBUTION OF BINDING ENERGY OF THE NOTCH RAM REGION TO THE CSL -TREFOIL DOMAIN AND THE MODE OF COMPETITION WITH THE VIRAL TRANSACTIVATOR EBNA2 *. *Journal of Biological Chemistry*, 285(9):6681–6692, February 2010.

[17] Sandro Keller, Carolyn Vargas, Huaying Zhao, Grzegorz Piszczek, Chad A. Brautigam, and Peter Schuck. High-Precision Isothermal Titration Calorimetry with Automated Peak-Shape Analysis. *Analytical Chemistry*, 84(11):5066–5073, June 2012. Publisher: American Chemical Society.

[18] Raphael Kopan and Ma Xenia G. Ilagan. The Canonical Notch Signaling Pathway: Unfolding the Activation Mechanism. *Cell*, 137(2):216–233, April 2009. Publisher: Elsevier.

[19] Rhett A. Kovall and Stephen C. Blacklow. Mechanistic insights into Notch receptor signaling from structural and biochemical studies. *Current Topics in Developmental Biology*, 92:31–71, 2010.

[20] Rhett A Kovall and Wayne A Hendrickson. Crystal structure of the nuclear effector of Notch signaling, CSL, bound to DNA. *The EMBO Journal*, 23(17):3441–3451, September 2004.

[21] Olga Y. Lubman, Ma Xenia G. Ilagan, Raphael Kopan, and Doug Barrick. Quantitative dissection of the Notch:CSL interaction: insights into the Notch-mediated transcriptional switch. *Journal of Molecular Biology*, 365(3):577–589, January 2007.

[22] J. S. Mumm, E. H. Schroeter, M. T. Saxena, A. Griesemer, X. Tian, D. J. Pan, W. J. Ray, and R. Kopan. A ligand-induced extracellular cleavage regulates gamma-secretase-like proteolytic activation of Notch1. *Molecular Cell*, 5(2):197–206, February 2000.

[23] Yunsun Nam, Piotr Sliz, Luyan Song, Jon C. Aster, and Stephen C. Blacklow. Structural Basis for Cooperativity in Recruitment of MAML Coactivators to Notch Transcription Complexes. *Cell*, 124(5):973–983, March 2006.

[24] Yunsun Nam, Andrew P. Weng, Jon C. Aster, and Stephen C. Blacklow. Structural requirements for assembly of the CSL.intracellular Notch1.Mastermind-like 1 transcriptional activation complex. *The Journal of Biological Chemistry*, 278(23):21232–21239, June 2003.

[25] Matthew Newville, Till Stensitzki, Daniel B. Allen, and Antonino Ingargiola. LMFIT: Non-Linear Least-Square Minimization and Curve-Fitting for Python. *Zenodo*, September 2014. Publisher: Zenodo ADS Bibcode: 2014zndo.....11813N.

[26] Kristen M. Ramsey and Doug Barrick. Unraveling paralog-specific Notch signaling through thermodynamics of ternary complex formation and transcriptional activation of chimeric receptors. *Protein Science*, 33(4):e4947, 2024. _eprint: https://onlinelibrary.wiley.com/doi/pdf/10.1002/pro.4947.

[27] J M Scholtz, S Marqusee, R L Baldwin, E J York, J M Stewart, M Santoro, and D W Bolen. Calorimetric determination of the enthalpy change for the alpha-helix to coil transition of an alanine peptide in water. *Proceedings of the National Academy of Sciences*, 88(7):2854–2858, April 1991. Publisher: Proceedings of the National Academy of Sciences.

[28] Kathryn Sherry. *STRUCTURAL AND THERMODYNAMIC ANALYSIS OF THE CONTRIBUTIONS OF THE INTRINSICALLY DISORDERED RAM REGION OF THE NOTCH RECEPTOR TO NOTCH SIGNALING*. PhD thesis, Johns Hopkins University, October 2015.

[29] Kathryn P. Sherry, Rahul K. Das, Rohit V. Pappu, and Doug Barrick. Control of transcriptional activity by design of charge patterning in the intrinsically disordered RAM region of the Notch receptor. *Proceedings of the National Academy of Sciences*, 114(44):E9243–E9252, October 2017.

[30] Kathryn P. Sherry, Scott E. Johnson, Christine L. Hatem, Ananya Majumdar, and Doug Barrick. Effects of Linker Length and Transient Secondary Structure Elements in the Intrinsically Disordered Notch RAM Region on Notch Signaling. *Journal of Molecular Biology*, 427(22):3587–3597, November 2015.

[31] Kumiko Tamura, Yoshihito Taniguchi, Shigeru Minoguchi, Takashi Sakai, Tin Tun, Takahisa Furukawa, and Tasuku Honjo. Physical interaction between a novel domain of the receptor Notch and the transcription factor RBP-J/Su(H). *Current Biology*, 5(12):1416–1423, December 1995.

[32] Lena Tveriakhina, Gustavo Scanavachi, Emily D. Egan, Ricardo Bango Da Cunha Correia, Alexandre P. Martin, Julia M. Rogers, Jeremy S. Yodh, Jon C. Aster, Tom Kirchhausen, and Stephen C. Blacklow. Temporal dynamics and stoichiometry in human Notch signaling from Notch synaptic complex formation to nuclear entry of the Notch intracellular domain. *Developmental Cell*, 59(11):1425–1438.e8, June 2024. Publisher: Elsevier.

[33] Sonia Vega, Olga Abian, and Adrian Velazquez-Campoy. A unified framework based on the binding polynomial for characterizing biological systems by isothermal titration calorimetry. *Methods (San Diego, Calif.)*, 76:99–115, April 2015.

[34] Jeffrey J. Wilson and Rhett A. Kovall. Crystal Structure of the CSL-Notch-Mastermind Ternary Complex Bound to DNA. *Cell*, 124(5):985–996, March 2006.

[35] Jeffries Wyman and Stanley J. Gill. *Binding and Linkage: Functional Chemistry of Biological Macromolecules*. University Science Books, 1990. Google-Books-ID: daxAKlHw7qQC.

[36] Binghan Zhou, Wanling Lin, Yaling Long, Yunkai Yang, Huan Zhang, Kongming Wu, and Qian Chu. Notch signaling pathway: architecture, disease, and therapeutics. *Signal Transduction and Targeted Therapy*, 7(1):1–33, March 2022. Publisher: Nature Publishing Group.